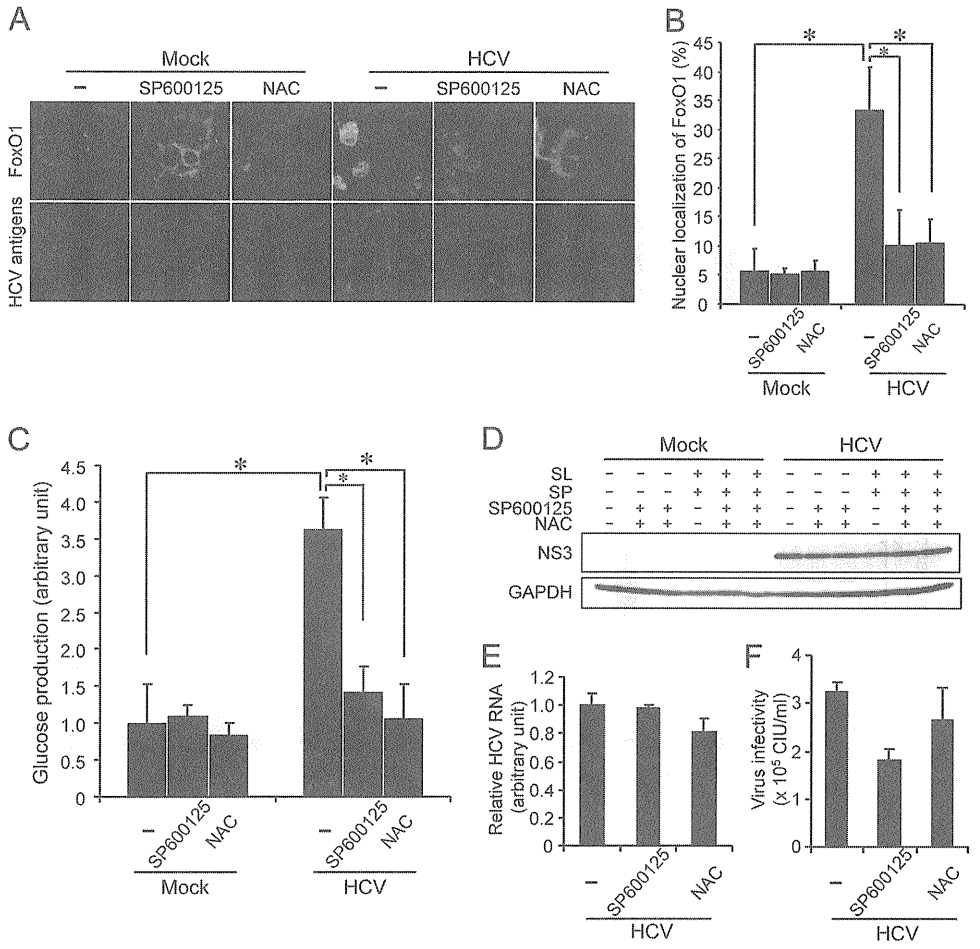

FIG. 6. HCV-induced JNK activation and ROS production are involved in FoxO1 nuclear accumulation and increased glucose production. (A) Subcellular localization of FoxO1 in HCV-infected cells and mock-infected controls with or without JNK inhibitor (SP600125 at 20 μM for 24 h) or antioxidant (NAC at 5 mM for 2 h) pretreatment at 5 dpi was examined by confocal microscopy. After fixation and permeabilization, the cells were incubated with an anti-FoxO1 rabbit monoclonal antibody followed by Alexa Fluor 488-conjugated goat anti-rabbit IgG (top) and with serum from an HCV-infected patient followed by Alexa Fluor 594-conjugated goat anti-human IgG (bottom). (B) The percentages of cells with FoxO1 nuclear localization were determined for HCV-infected cells and mock-infected controls with or without SP600125 or NAC pretreatment. Data represent means ± SEM of data from two independent experiments. *, $P < 0.01$. (C) Extracellular glucose production was measured in HCV-infected cells and mock-infected controls with or without SP600125 or NAC pretreatment at 7 dpi and normalized to total cellular protein expression levels. Data represent means ± SEM of data from two independent experiments, and the value for the control cells was arbitrarily expressed as 1.0. *, $P < 0.01$. (D) Cellular expression levels of NS3 in HCV-infected cells and mock-infected control cells with or without sodium lactate (SL), sodium pyruvate (SP), SP600125, or NAC are shown. The amounts of GAPDH were measured as an internal control to verify equal amounts of sample loading. (E) Amounts of HCV RNA were measured by quantitative RT-PCR analysis of HCV-infected cells treated with SP600125 or NAC or left untreated at 6 dpi. The amounts were normalized to GAPDH mRNA expression levels. Data represent means ± SEM of data from two independent experiments, and the value for the nontreated HCV-infected cells was arbitrarily expressed as 1.0. (F) Virus infectivity in the culture supernatants of HCV-infected cells treated with SP600125 or NAC or left untreated at 6 dpi was measured. Data represent means ± SEM of data from two independent experiments. CIU, cell-infecting units.

hand, the nuclear accumulation of FoxO1 was clearly observed in approximately 35% of HCV-infected cells at 5 dpi. The treatment of HCV-infected cells with a JNK inhibitor (SP600125 at 20 μM for 24 h) or an antioxidant (NAC at 5 mM for 2 h) significantly inhibited HCV-induced FoxO1 nuclear accumulation.

To further verify the role played by JNK activation and ROS production in HCV-induced hepatic gluconeogenesis, the glucose production in SP600125- or NAC-treated HCV-infected cells was assessed. Treatment with SP600125 or NAC significantly impaired the HCV-induced increased glucose production at 7 dpi (Fig. 6C) but did not affect the overall abundance of the HCV NS3 protein (Fig. 6D). We also examined the possible effects of SP600125 or NAC on HCV RNA replication and infectious-virus production. The results obtained revealed that treatment with SP600125 (20 μM for 24 h) or NAC (5 mM for 2 h) barely affected HCV RNA replication (Fig. 6E). On the other hand, we noted a tendency for infectious-virus production to be only slightly suppressed by SP600125 but not by NAC (Fig. 6F). A short-term inhibition of glucose production might not sufficiently affect HCV RNA replication or virus production.

Taken together, these results indicate that ROS-mediated JNK activation plays a key role in the suppression of FoxO1

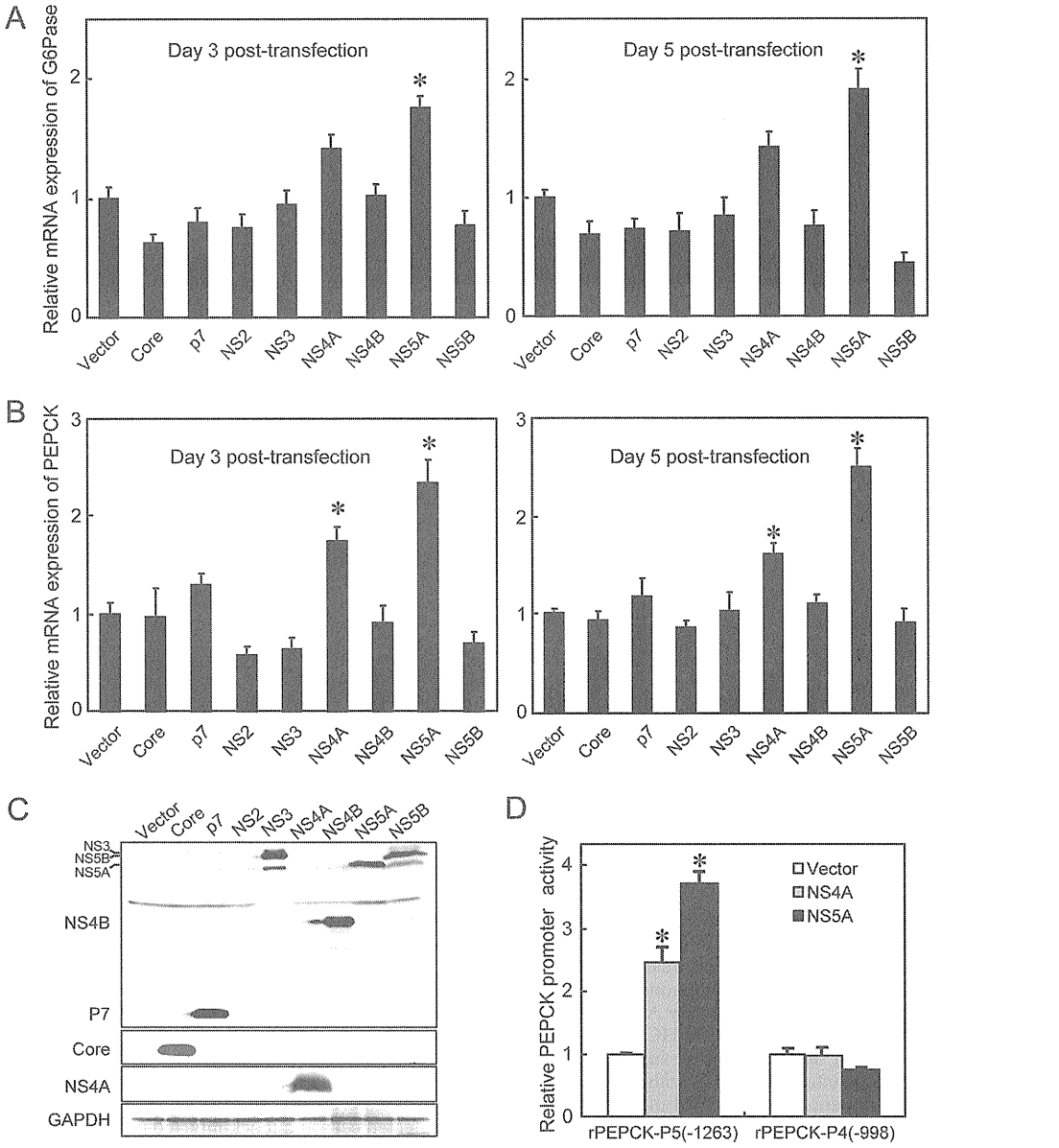

FIG. 7. HCV NS5A is involved in increased mRNA expression levels for G6Pase and PEPCK. Huh-7.5 cells were transfected with the indicated HCV viral protein expression plasmids. (A and B) At 3 and 5 days posttransfection, quantitative RT-PCR analyses of mRNA for G6Pase (A) and PEPCK (B) were conducted, and the results were normalized to β-glucuronidase mRNA expression levels. Data represent means ± SEM of data from three independent experiments, and the values for the control cells were arbitrarily expressed as 1.0. *, $P < 0.01$ compared with the control. (C) At 3 days posttransfection, the expression levels of each of the HCV proteins were examined by immunoblot analysis using antibodies against c-Myc, core, NS4A, and GAPDH. The amounts of GAPDH served as an internal control to verify equal amounts of sample loading. (D) NS5A and NS4A enhance PEPCK promoter activity. NS5A and NS4A expression plasmids were each cotransfected with rPEPCK-P5(−1263)-pGL3basic or rPEPCK-P4(−998)-pGL3basic in Huh-7.5 cells. At 48 h after transfection, the PEPCK promoter activities were measured by using a luciferase reporter assay. Data represent means ± SEM of data from three independent experiments, and the values for the control cells were arbitrarily expressed as 1.0. *, $P < 0.05$ compared with the control.

phosphorylation, the nuclear accumulation of FoxO1, and the enhancement of glucose production in HCV-infected cells.

HCV NS5A is involved in the enhancement of glucose production. To examine which HCV protein(s) is involved in the enhancement of gluconeogenesis, expression constructs of each of the HCV viral proteins were transfected into Huh-7.5 cells, and the gene expression levels of PEPCK and G6Pase were examined by real-time quantitative RT-PCR analysis. We observed that NS5A significantly promoted G6Pase gene expression (Fig. 7A). Moreover, both the NS5A and NS4A proteins significantly enhanced PEPCK gene expression at 3 and 5 days posttransfection, respectively (Fig. 7B). The expression of each of the HCV proteins except NS2 was verified by immunoblot analysis (Fig. 7C). NS2 was reported previously to be unstable and rapidly degraded by the proteasome (22).

Next, we performed a luciferase reporter assay to examine

the possible effects of NS5A and NS4A on PEPCK promoter activities. The construct rPEPCK-P5(−1263)-pGL3basic carries 1,263 bp of the PEPCK 5′-flanking region (−1263 PEPCK) and is used to monitor PEPCK promoter activity. The results demonstrated that the levels of PEPCK promoter activities were significantly higher in both NS5A- and NS4A-expressing cells than in the control cells (Fig. 7D). Interestingly, when the region of the PEPCK promoter from positions −1263 to −998 was deleted, the activation of PEPCK promoter activity in cells expressing NS5A and NS4A was abolished. These results confirmed that NS5A and NS4A activate the PEPCK promoter, leading to an increase in PEPCK mRNA expression levels. Database searches of the deleted sequence did not reveal any potential binding sequences for transcription factors (data not shown).

Recently reported data suggest that ROS production is induced in NS5A-expressing cells (17) or in hepatocytes of NS5A transgenic mice (68). We therefore sough to determine whether NS5A contributes to increased hepatic gluconeogenesis through the induction of ROS production. The NS5A expression plasmid was transfected into Huh-7.5 cells, and ROS production was assessed by MitoSOX at 3 days posttransfection. As shown in Fig. 8A and B, approximately 30% of NS5A-expressing cells displayed a much stronger signal than that observed for vector-transfected control cells.

We then examined whether NS5A mediated JNK/c-Jun activation and FoxO1 phosphorylation inhibition. The results obtained revealed that both the phosphorylation level at Ser63 and the total expression level of c-Jun were upregulated in NS5A-expressing cells compared to the control cells transfected with the vector plasmid or cells expressing the other HCV proteins (Fig. 8C and D, top two panels). Concomitantly, FoxO1 phosphorylation at Ser319 was clearly suppressed in NS5A- and NS4A-expressing cells compared to the control cells (Fig. 8C, compare lanes 6, 5, and 1, respectively, in the third panel). NS4A, a small protein of ca. 7 kDa, forms a stable complex with NS3 to function as a cofactor for NS3 serine protease and RNA helicase activities (51). We previously reported that NS4A caused mitochondrial damage when expressed alone but not when coexpressed with NS3 (47). We therefore speculated that the otherwise observed decrease in FoxO1 phosphorylation levels in NS4A-expressing cells might be canceled when NS4A is coexpressed with NS3. To verify this notion, we tested FoxO1 phosphorylation in cells coexpressing NS3 and NS4A. As had been expected, FoxO1 phosphorylation levels did not differ between NS3/4A-coexpressing cells and vector-transfected control cells (Fig. 8C, compare lanes 4 and 1, respectively).

Notably, we observed that the HCV core protein did not alter the phosphorylation status of c-Jun and FoxO1 (Fig. 8C, compare lanes 1 and 2), with the result being consistent with what was observed for gene expression levels of PEPCK and G6Pase in HCV core-expressing cells (Fig. 7A and B). These results imply that core is not primarily involved in HCV-induced increased gluconeogenesis under our experimental conditions. Similarly, other HCV nonstructural proteins, such as NS4B and NS5B, did not significantly influence the phosphorylation status of c-Jun and FoxO1 (Fig. 8D).

In order to further verify the effect of NS5A on the nuclear accumulation of FoxO1, we examined the subcellular localization of FoxO1 in NS5A-expressing cells by indirect immunofluorescence staining. As shown in Fig. 8E and F, the nuclear accumulation of FoxO1 was clearly observed for approximately 25% of NS5A-expressing cells but not the vector-transfected control. These results suggest that NS5A activates the JNK/c-Jun signaling pathway via increased ROS production, which results in the decreased phosphorylation and nuclear accumulation of FoxO1.

Finally, we examined the effects of NS5A and NS4A on glucose production. As shown in Fig. 9, the amounts of glucose were significantly increased in culture supernatants of NS5A- and NS4A-expressing cells, compared with the amounts of glucose in control cells, at 5 days posttransfection. Again, it is reasonable to assume that the observed increase in glucose production in NS4A-expressing cells might be canceled when NS4A is coexpressed with NS3.

These results collectively suggest that NS5A plays a role, at least to some extent, in the HCV-induced enhancement of hepatic gluconeogenesis.

DISCUSSION

Hepatocytes play an important role in maintaining plasma glucose homeostasis by adjusting the balance between hepatic glucose production and utilization via the gluconeogenic and glycolytic pathways, respectively. We previously reported that HCV suppresses cellular glucose uptake by downregulating the surface expression of the glucose transporters GLUT1 and GLUT2 (37). In this study, we have demonstrated that HCV promotes FoxO1-mediated hepatic gluconeogenesis, as evidenced by the increased accumulation of FoxO1 in the nucleus via the reduction of its phosphorylation status (Fig. 3 and 6A and B), which leads to increased PEPCK and G6Pase gene expression levels (Fig. 1A and B) and the subsequent upregulation of G6P and glucose production (Fig. 2). Moreover, our results indicate that HCV-induced ROS production causes JNK activation, which results in the decreased phosphorylation and nuclear accumulation of FoxO1, leading eventually to increased glucose production (Fig. 4 to 6). Our results thus suggest that FoxO1 is a prime transcription factor in the HCV-mediated progression of hepatic gluconeogenesis through an ROS/JNK-dependent mechanism, as summarized in the schema in Fig. 10. Our results also suggest that HCV NS5A plays a role in enhanced hepatic gluconeogenesis by promoting ROS production and JNK activation (Fig. 7 to 9). In line with our observations, the NS5A-mediated induction of ROS production (68) and JNK activation (49) was reported previously by other investigators.

Increasing evidence suggests that mitochondrial dysfunction is causative of insulin resistance and type 2 diabetes. Mitochondrial dysfunction causes the upregulation of PEPCK and G6Pase, leading to increased gluconeogenesis and insulin resistance (42, 46). We previously reported that HCV causes mitochondrial damage and mitochondrion-mediated apoptosis (14, 47). Our current data further support the concept that altered mitochondrial function plays a role in the development of increased glucose production in hepatocytes.

We and other groups have reported that HCV infection increases the production of mitochondrial ROS, which plays an important role in the development and progression of inflam-

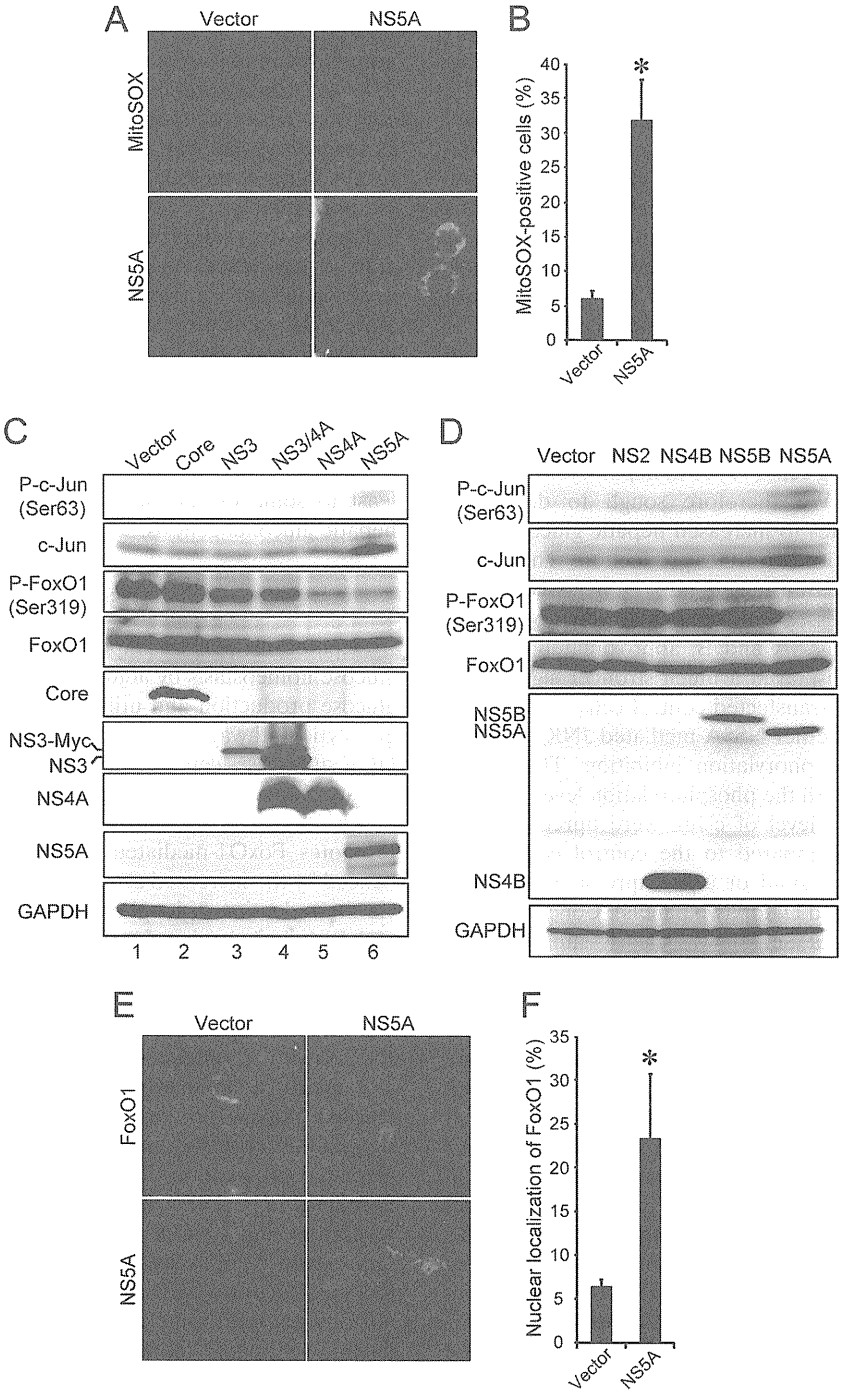

FIG. 8. HCV NS5A is involved in increased ROS production, JNK activation, FoxO1 phosphorylation suppression, and FoxO1 nuclear accumulation. (A) NS5A promotes ROS production. Huh-7.5 cells transfected with an NS5A expression plasmid or the empty control (vector) were incubated with MitoSOX (top) at 3 days posttransfection and then stained for NS5A by using anti-NS5A mouse monoclonal antibody, followed by FITC-conjugated goat anti-mouse IgG (bottom). (B) Quantification of MitoSOX-stained cells. The percentages of cells stained with MitoSOX were determined for NS5A-expressing cells and control cells. Data represent means ± SEM of data from two independent experiments. *, $P < 0.01$. (C and D) HCV NS5A activates c-Jun phosphorylation and suppresses FoxO1 phosphorylation. Huh-7.5 cells transfected with the indicated HCV viral protein expression plasmids were harvested at 3 days posttransfection, and the whole-cell lysates were subjected to immunoblot analysis using antibodies against phospho-c-Jun (Ser63), c-Jun, phospho-FoxO1 (Ser319), FoxO1, GAPDH, core, NS3, NS4A, and NS5A (C) or c-Myc (D). The amounts of GAPDH were measured as an internal control to verify equal amounts of sample loading. (E) NS5A facilitates FoxO1 nuclear accumulation. Huh-7.5 cells transfected with an NS5A expression plasmid or the empty control (vector) were fixed and permeabilized at 3 days posttransfection. The cells were incubated with an anti-FoxO1 rabbit monoclonal antibody followed by Alexa Fluor 488-conjugated goat anti-rabbit IgG (top) or with anti-NS5A mouse monoclonal antibody followed by Alexa Fluor 594-conjugated goat anti-mouse IgG (bottom). (F) The percentages of cells with a nuclear localization of FoxO1 were determined for NS5A-expressing cells and control cells. Data represent means ± SEM of data from two independent experiments. *, $P < 0.01$.

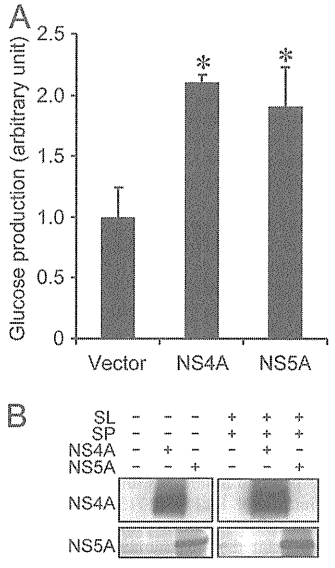

FIG. 9. HCV NS5A and NS4A enhance glucose production. (A) Huh-7.5 cells were transfected with either an NS5A or NS4A expression plasmid. At 5 days posttransfection, extracellular glucose production was measured and normalized to the total cellular protein expression level. Data represent means ± SEM of data from two independent experiments, and the values for the control cells were arbitrarily expressed as 1.0. *, $P < 0.05$ compared with the control. (B) Cellular expression levels of NS4A and NS5A in the absence and presence of sodium lactate (SL) and sodium pyruvate (SP) are shown.

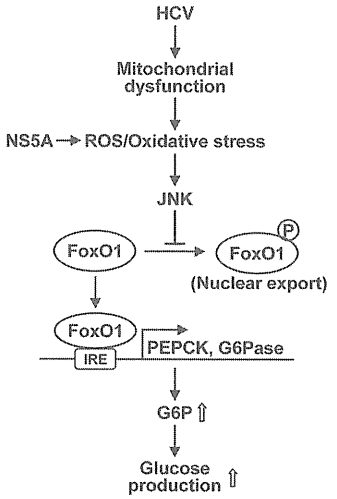

FIG. 10. Schematic representation of the HCV-dysregulated hepatic gluconeogenesis signaling pathway. HCV induces mitochondrial dysfunction (14). This results in increased ROS production and JNK activation, which induces the nuclear accumulation of FoxO1 by reducing its phosphorylation status. Consequently, PEPCK and G6Pase gene expressions are upregulated, leading to an upregulation of G6P and glucose production. NS5A plays a role in HCV-induced gluconeogenesis via the induction of ROS production. IRE, insulin response element.

matory liver disease mediated by HCV (12, 14). Increased mitochondrial ROS generation was also shown previously to be an underlying mediator of multiple forms of insulin resistance, including inflammation- or glucocorticoid-induced insulin resistance (27, 29). Moreover, a significant correlation was observed between oxidative stress and insulin resistance in patients infected with HCV genotype 1 or 2 (44). ROS have also been shown to regulate the activity of the FoxO transcription factor by posttranslational modifications, including phosphorylation (21), deacetylation (8), and ubiquitylation (67).

Although this study showed that JNK induces the nuclear accumulation of FoxO1 by reducing its phosphorylation status under oxidative stress conditions in HCV-infected cells, the precise mechanism(s) of the interplay between JNK and FoxO1 still remains to be addressed. It was reported previously that activated JNK phosphorylates IRS-1 at Ser307, which results in attenuated insulin signal transduction through the inhibition of the tyrosine phosphorylation of IRS-1 (1). Akt is a major downstream signaling protein for insulin/IRS-1 signaling and is activated through its phosphorylation on Thr308 and Ser473, the latter of which is believed to be more crucial (53). Therefore, an impairment of the insulin/IRS-1 signaling pathway should involve the downregulation of Akt phosphorylation. However, our present data showed that Akt phosphorylation on Ser473 was upregulated in HCV-infected cells at 4 and 6 dpi (Fig. 3B), suggesting that an Akt-independent pathway is involved in the JNK-mediated suppression of FoxO1 phosphorylation. Regarding this connection, it should be noted that the 14-3-3 protein, a binding partner for phosphorylated FoxO1 that mediates its nuclear export (72), is phosphorylated by JNK and that the phosphorylated 14-3-3 protein releases its binding partners, which would facilitate the nuclear accumulation of FoxO (63, 65, 70). Further studies are needed to elucidate this issue.

Another trigger that causes excessive JNK activation and insulin resistance is endoplasmic reticulum (ER) stress (28, 48). Several previous studies reported that HCV infection induces ER stress (34, 55). Under our experimental conditions, however, we did not detect significant ER stress in HCV-infected cells (14). It is thus likely that ER stress was not the primary cause of the increased gluconeogenesis in our experimental system using Huh-7.5 cells and the P-47 strain of HCV J6/JFH-1 (9, 14).

Notably, our present data showed that cells harboring the SGR or FGR and HCV-infected cells produced greater amounts of glucose than did the control cells (Fig. 2A); however, the changes in the phosphorylation status of FoxO1 and JNK in SGR- and FGR-harboring cells were not so significant compared to those in virus-infected cells (data not shown). One of the reasons for this difference is that SGR- and FGR-harboring cells were obtained through a longer cultivation in a selection medium for a month or more and that the balance of host gene induction may be somewhat different from that in virus-infected cells. Therefore, it is possible that, in addition to the JNK-FoxO1 pathway, another signaling pathway(s) is involved in the increased gluconeogenesis in SGR- and FGR-harboring cells. Studies on this issue are now under way in our laboratory.

We observed that HCV infection modulated, either positively or negatively, the transcription of the PEPCK, G6Pase, and GK genes at 3 to 5 dpi (Fig. 1). Virus infection, in general, causes dynamically changing induction and the suppression of a wide variety of host genes. For example, expression levels of certain genes, such as interferon genes, increase during an

early phase of virus infection, e.g., at 1 dpi, but return to normal levels within a few days in a cell culture system. On the other hand, the virus-infection-induced expression of other genes, such as the extracellular signal-regulated kinase (ERK) gene, remains for a prolonged period of time (data not shown). Also, some of the gene products induced in the acute phase may suppress the expression of other genes. Under these balanced conditions, it is quite possible that certain genes are induced only at a later time, e.g., 3 to 5 dpi, but not immediately after virus infection.

It was reported previously that HCV core protein-expressing transgenic mice exhibit marked insulin resistance by inhibiting IRS-1 tyrosine phosphorylation and Akt phosphorylation (45, 58). However, our present results showed that HCV NS5A, but not the core protein, was associated with increased gluconeogenesis. Moreover, it was recently reported that HCV infection significantly inhibited cellular glucose levels at 10 dpi (69), which is quite the opposite of what we observed in the present study. These results collectively suggest the possibility that multiple pathways are involved in glucose metabolism in HCV-infected cells. Also, the possible effect(s) of the dysregulation of hepatic gluconeogenesis on the HCV life cycle needs to be clarified.

In conclusion, our present results collectively suggest that HCV promotes hepatic gluconeogenesis, resulting in increased glucose production in hepatocytes via an NS5A-mediated, FoxO1-dependent pathway.

ACKNOWLEDGMENTS

We are grateful to C. M. Rice (Rockefeller University, New York, NY) for providing Huh-7.5 cells and pFL-J6/JFH1, R. Bartenschlager (University of Heidelberg, Heidelberg, Germany) for providing an HCV subgenomic RNA replicon (pFK5B/2884Gly), and N. Kato (Okayama University, Okayama, Japan) for providing an HCV full-length RNA replicon (pON/C-5B). We also thank T. Adachi (Kyoto Prefectural University of Medicine, Kyoto, Japan), K. Igarashi, K. Kashikura, and A. Suzuki (Keio University, Yamagata, Japan) for their technical assistance.

This work was supported in part by grants-in-aid for research on hepatitis from the Ministry of Health, Labor, and Welfare, Japan, and the Japan Initiative for Global Research Network on Infectious Diseases (J-GRID) program of the Ministry of Education, Culture, Sports, Science, and Technology, Japan. This study was also carried out as part of the Global Center of Excellence program of the Kobe University Graduate School of Medicine and the Science and Technology Research Partnership for Sustainable Development (SATREPS) program of the Japan Science and Technology Agency (JST) and the Japan International Cooperation Agency (JICA).

REFERENCES

1. **Aguirre, V., T. Uchida, L. Yenush, R. Davis, and M. F. White.** 2000. The c-Jun NH(2)-terminal kinase promotes insulin resistance during association with insulin receptor substrate-1 and phosphorylation of Ser(307). J. Biol. Chem. **275:**9047–9054.
2. **Alaei, M., and F. Negro.** 2008. Hepatitis C virus and glucose and lipid metabolism. Diabetes Metab. **34:**692–700.
3. **Aytug, S., D. Reich, L. E. Sapiro, D. Bernstein, and N. Begum.** 2003. Impaired IRS-1/PI3-kinase signaling in patients with HCV: a mechanism for increased prevalence of type 2 diabetes. Hepatology **38:**1384–1392.
4. **Banerjee, A., K. Meyer, B. Mazumdar, R. B. Ray, and R. Ray.** 2010. Hepatitis C virus differentially modulates activation of forkhead transcription factors and insulin-induced metabolic gene expression. J. Virol. **84:**5936–5946.
5. **Baron, A. D., L. Schaeffer, P. Shragg, and O. G. Kolterman.** 1987. Role of hyperglucagonemia in maintenance of increased rates of hepatic glucose output in type II diabetics. Diabetes **36:**274–283.
6. **Bennett, B. L., et al.** 2001. SP600125, an anthrapyrazolone inhibitor of Jun N-terminal kinase. Proc. Natl. Acad. Sci. U. S. A. **98:**13681–13686.
7. **Blight, K. J., J. A. McKeating, and C. M. Rice.** 2002. Highly permissive cell lines for subgenomic and genomic hepatitis C virus RNA replication. J. Virol. **76:**13001–13014.
8. **Brunet, A., et al.** 2004. Stress-dependent regulation of FOXO transcription factors by the SIRT1 deacetylase. Science **303:**2011–2015.
9. **Bungyoku, Y., et al.** 2009. Efficient production of infectious hepatitis C virus with adaptive mutations in cultured hepatoma cells. J. Gen. Virol. **90:**1681–1691.
10. **Burdette, D., M. Olivarez, and G. Waris.** 2010. Activation of transcription factor Nrf2 by hepatitis C virus induces the cell-survival pathway. J. Gen. Virol. **91:**681–690.
11. **Caronia, S., et al.** 1999. Further evidence for an association between non-insulin-dependent diabetes mellitus and chronic hepatitis C virus infection. Hepatology **30:**1059–1063.
12. **Choi, J., and J. H. Ou.** 2006. Mechanisms of liver injury. III. Oxidative stress in the pathogenesis of hepatitis C virus. Am. J. Physiol. Gastrointest. Liver Physiol. **290:**G847–G851.
13. **Clore, J. N., J. Stillman, and H. Sugerman.** 2000. Glucose-6-phosphatase flux in vitro is increased in type 2 diabetes. Diabetes **49:**969–974.
14. **Deng, L., et al.** 2008. Hepatitis C virus infection induces apoptosis through a Bax-triggered, mitochondrion-mediated, caspase 3-dependent pathway. J. Virol. **82:**10375–10385.
15. **Deng, L., et al.** 2006. NS3 protein of hepatitis C virus associates with the tumour suppressor p53 and inhibits its function in an NS3 sequence-dependent manner. J. Gen. Virol. **87:**1703–1713.
16. **Diamond, D. L., et al.** 2010. Temporal proteome and lipidome profiles reveal hepatitis C virus-associated reprogramming of hepatocellular metabolism and bioenergetics. PLoS Pathog. **6:**e1000719.
17. **Dionisio, N., et al.** 2009. Hepatitis C virus NS5A and core proteins induce oxidative stress-mediated calcium signalling alterations in hepatocytes. J. Hepatol. **50:**872–882.
18. **Doi, H., C. Apichartpiyakul, K. I. Ohba, M. Mizokami, and H. Hotta.** 1996. Hepatitis C virus (HCV) subtype prevalence in Chiang Mai, Thailand, and identification of novel subtypes of HCV major type 6. J. Clin. Microbiol. **34:**569–574.
19. **Dunning, B. E., and J. E. Gerich.** 2007. The role of alpha-cell dysregulation in fasting and postprandial hyperglycemia in type 2 diabetes and therapeutic implications. Endocr. Rev. **28:**253–283.
20. **Eslam, M., M. A. Khattab, and S. A. Harrison.** 2011. Insulin resistance and hepatitis C: an evolving story. Gut **60:**1139–1151.
21. **Essers, M. A., et al.** 2004. FOXO transcription factor activation by oxidative stress mediated by the small GTPase Ral and JNK. EMBO J. **23:**4802–4812.
22. **Franck, N., J. Le Seyec, C. Guguen-Guillouzo, and L. Erdtmann.** 2005. Hepatitis C virus NS2 protein is phosphorylated by the protein kinase CK2 and targeted for degradation to the proteasome. J. Virol. **79:**2700–2708.
23. **Galossi, A., R. Guarisco, L. Bellis, and C. Puoti.** 2007. Extrahepatic manifestations of chronic HCV infection. J. Gastrointestin. Liver Dis. **16:**65–73.
24. **Gottwein, J. M., et al.** 2009. Development and characterization of hepatitis C virus genotype 1-7 cell culture systems: role of CD81 and scavenger receptor class B type I and effect of antiviral drugs. Hepatology **49:**364–377.
25. **Gross, D. N., A. P. van den Heuvel, and M. J. Birnbaum.** 2008. The role of FoxO in the regulation of metabolism. Oncogene **27:**2320–2336.
26. **Hirota, K., et al.** 2008. A combination of HNF-4 and Foxo1 is required for reciprocal transcriptional regulation of glucokinase and glucose-6-phosphatase genes in response to fasting and feeding. J. Biol. Chem. **283:**32432–32441.
27. **Hoehn, K. L., et al.** 2009. Insulin resistance is a cellular antioxidant defense mechanism. Proc. Natl. Acad. Sci. U. S. A. **106:**17787–17792.
28. **Hotamisligil, G. S.** 2005. Role of endoplasmic reticulum stress and c-Jun NH2-terminal kinase pathways in inflammation and origin of obesity and diabetes. Diabetes **54**(Suppl. 2)**:**S73–S78.
29. **Houstis, N., E. D. Rosen, and E. S. Lander.** 2006. Reactive oxygen species have a causal role in multiple forms of insulin resistance. Nature **440:**944–948.
30. **Huang, H., and D. J. Tindall.** 2007. Dynamic FoxO transcription factors. J. Cell Sci. **120:**2479–2487.
31. **Ikeda, M., et al.** 2005. Efficient replication of a full-length hepatitis C virus genome, strain O, in cell culture, and development of a luciferase reporter system. Biochem. Biophys. Res. Commun. **329:**1350–1359.
32. **Inubushi, S., et al.** 2008. Hepatitis C virus NS5A protein interacts with and negatively regulates the non-receptor protein tyrosine kinase Syk. J. Gen. Virol. **89:**1231–1242.
33. **Iynedjian, P. B., et al.** 1989. Differential expression and regulation of the glucokinase gene in liver and islets of Langerhans. Proc. Natl. Acad. Sci. U. S. A. **86:**7838–7842.
34. **Joyce, M. A., et al.** 2009. HCV induces oxidative and ER stress, and sensitizes infected cells to apoptosis in SCID/Alb-uPA mice. PLoS Pathog. **5:**e1000291.
35. **Kamata, H., et al.** 2005. Reactive oxygen species promote TNFalpha-induced death and sustained JNK activation by inhibiting MAP kinase phosphatases. Cell **120:**649–661.
36. **Karpac, J., and H. Jasper.** 2009. Insulin and JNK: optimizing metabolic homeostasis and lifespan. Trends Endocrinol. Metab. **20:**100–106.
37. **Kasai, D., et al.** 2009. HCV replication suppresses cellular glucose uptake

through down-regulation of cell surface expression of glucose transporters. J. Hepatol. **50:**883–894.
38. **Kops, G. J., and B. M. Burgering.** 1999. Forkhead transcription factors: new insights into protein kinase B (c-akt) signaling. J. Mol. Med. **77:**656–665.
39. **Lindenbach, B. D., et al.** 2005. Complete replication of hepatitis C virus in cell culture. Science **309:**623–626.
40. **Lindenbach, B. D., and C. M. Rice.** 2005. Unravelling hepatitis C virus replication from genome to function. Nature **436:**933–938.
41. **Lohmann, V., F. Korner, A. Dobierzewska, and R. Bartenschlager.** 2001. Mutations in hepatitis C virus RNAs conferring cell culture adaptation. J. Virol. **75:**1437–1449.
42. **Lowell, B. B., and G. I. Shulman.** 2005. Mitochondrial dysfunction and type 2 diabetes. Science **307:**384–387.
43. **Mehta, S. H., et al.** 2000. Prevalence of type 2 diabetes mellitus among persons with hepatitis C virus infection in the United States. Ann. Intern. Med. **133:**592–599.
44. **Mitsuyoshi, H., et al.** 2008. Evidence of oxidative stress as a cofactor in the development of insulin resistance in patients with chronic hepatitis C. Hepatol. Res. **38:**348–353.
45. **Miyamoto, H., et al.** 2007. Involvement of the PA28gamma-dependent pathway in insulin resistance induced by hepatitis C virus core protein. J. Virol. **81:**1727–1735.
46. **Morino, K., K. F. Petersen, and G. I. Shulman.** 2006. Molecular mechanisms of insulin resistance in humans and their potential links with mitochondrial dysfunction. Diabetes **55**(Suppl. 2)**:**S9–S15.
47. **Nomura-Takigawa, Y., et al.** 2006. Non-structural protein 4A of hepatitis C virus accumulates on mitochondria and renders the cells prone to undergoing mitochondria-mediated apoptosis. J. Gen. Virol. **87:**1935–1945.
48. **Ozcan, U., et al.** 2004. Endoplasmic reticulum stress links obesity, insulin action, and type 2 diabetes. Science **306:**457–461.
49. **Park, K. J., et al.** 2003. Hepatitis C virus NS5A protein modulates c-Jun N-terminal kinase through interaction with tumor necrosis factor receptor-associated factor 2. J. Biol. Chem. **278:**30711–30718.
50. **Puigserver, P., et al.** 2003. Insulin-regulated hepatic gluconeogenesis through FOXO1-PGC-1alpha interaction. Nature **423:**550–555.
51. **Reed, K. E., and C. M. Rice.** 2000. Overview of hepatitis C virus genome structure, polyprotein processing, and protein properties. Curr. Top. Microbiol. Immunol. **242:**55–84.
52. **Rozance, P. J., et al.** 2008. Chronic late-gestation hypoglycemia upregulates hepatic PEPCK associated with increased PGC1alpha mRNA and phosphorylated CREB in fetal sheep. Am. J. Physiol. Endocrinol. Metab. **294:** E365–E370.
53. **Sale, E. M., and G. J. Sale.** 2008. Protein kinase B: signalling roles and therapeutic targeting. Cell. Mol. Life Sci. **65:**113–127.
54. **Schmoll, D., et al.** 2000. Regulation of glucose-6-phosphatase gene expression by protein kinase Balpha and the forkhead transcription factor FKHR. Evidence for insulin response unit-dependent and -independent effects of insulin on promoter activity. J. Biol. Chem. **275:**36324–36333.
55. **Sekine-Osajima, Y., et al.** 2008. Development of plaque assays for hepatitis C virus-JFH1 strain and isolation of mutants with enhanced cytopathogenicity and replication capacity. Virology **371:**71–85.
56. **Seo, H. Y., et al.** 2010. Endoplasmic reticulum stress-induced activation of activating transcription factor 6 decreases cAMP-stimulated hepatic gluconeogenesis via inhibition of CREB. Endocrinology **151:**561–568.
57. **Shepard, C. W., L. Finelli, and M. J. Alter.** 2005. Global epidemiology of hepatitis C virus infection. Lancet Infect. Dis. **5:**558–567.
58. **Shintani, Y., et al.** 2004. Hepatitis C virus infection and diabetes: direct involvement of the virus in the development of insulin resistance. Gastroenterology **126:**840–848.
59. **Simmonds, P., et al.** 2005. Consensus proposals for a unified system of nomenclature of hepatitis C virus genotypes. Hepatology **42:**962–973.
60. **Soga, T., et al.** 2006. Differential metabolomics reveals ophthalmic acid as an oxidative stress biomarker indicating hepatic glutathione consumption. J. Biol. Chem. **281:**16768–16776.
61. **Soga, T., et al.** 2009. Metabolomic profiling of anionic metabolites by capillary electrophoresis mass spectrometry. Anal. Chem. **81:**6165–6174.
62. **Streeper, R. S., et al.** 1997. A multicomponent insulin response sequence mediates a strong repression of mouse glucose-6-phosphatase gene transcription by insulin. J. Biol. Chem. **272:**11698–11701.
63. **Sunayama, J., F. Tsuruta, N. Masuyama, and Y. Gotoh.** 2005. JNK antagonizes Akt-mediated survival signals by phosphorylating 14-3-3. J. Cell Biol. **170:**295–304.
64. **Takashima, M., et al.** 2010. Role of KLF15 in regulation of hepatic gluconeogenesis and metformin action. Diabetes **59:**1608–1615.
65. **Tsuruta, F., et al.** 2004. JNK promotes Bax translocation to mitochondria through phosphorylation of 14-3-3 proteins. EMBO J. **23:**1889–1899.
66. **van der Horst, A., and B. M. Burgering.** 2007. Stressing the role of FoxO proteins in lifespan and disease. Nat. Rev. Mol. Cell Biol. **8:**440–450.
67. **van der Horst, A., et al.** 2006. FOXO4 transcriptional activity is regulated by monoubiquitination and USP7/HAUSP. Nat. Cell Biol. **8:**1064–1073.
68. **Wang, A. G., et al.** 2009. Non-structural 5A protein of hepatitis C virus induces a range of liver pathology in transgenic mice. J. Pathol. **219:**253–262.
69. **Woodhouse, S. D., et al.** 2010. Transcriptome sequencing, microarray, and proteomic analyses reveal cellular and metabolic impact of hepatitis C virus infection in vitro. Hepatology **52:**443–453.
70. **Yoshida, K., T. Yamaguchi, T. Natsume, D. Kufe, and Y. Miki.** 2005. JNK phosphorylation of 14-3-3 proteins regulates nuclear targeting of c-Abl in the apoptotic response to DNA damage. Nat. Cell Biol. **7:**278–285.
71. **Zhang, S., J. Liu, G. MacGibbon, M. Dragunow, and G. J. Cooper.** 2002. Increased expression and activation of c-Jun contributes to human amylin-induced apoptosis in pancreatic islet beta-cells. J. Mol. Biol. **324:**271–285.
72. **Zhao, X., et al.** 2004. Multiple elements regulate nuclear/cytoplasmic shuttling of FOXO1: characterization of phosphorylation- and 14-3-3-dependent and -independent mechanisms. Biochem. J. **378:**839–849.

LIPIDS IN HEALTH AND DISEASE

RESEARCH Open Access

LXR agonist increases apoE secretion from HepG2 spheroid, together with an increased production of VLDL and apoE-rich large HDL

Makoto Kurano[1], Naoyuki Iso-O[5], Masumi Hara[6], Nobukazu Ishizaka[2], Kyoji Moriya[3], Kazuhiko Koike[4] and Kazuhisa Tsukamoto[1,7*]

Abstract

Background: The physiological regulation of hepatic apoE gene has not been clarified, although the expression of apoE in adipocytes and macrophages has been known to be regulated by LXR.

Methods and Results: We investigated the effect of TO901317, a LXR agonist, on hepatic apoE production utilizing HepG2 cells cultured in spheroid form, known to be more differentiated than HepG2 cells in monolayer culture. Spheroid HepG2 cells were prepared in alginate-beads. The secretions of albumin, apoE and apoA-I from spheroid HepG2 cells were significantly increased compared to those from monolayer HepG2 cells, and these increases were accompanied by increased mRNA levels of apoE and apoA-I. Several nuclear receptors including LXRα also became abundant in nuclear fractions in spheroid HepG2 cells. Treatment with TO901317 significantly increased apoE protein secretion from spheroid HepG2 cells, which was also associated with the increased expression of apoE mRNA. Separation of the media with FPLC revealed that the production of apoE-rich large HDL particles were enhanced even at low concentration of TO901317, and at higher concentration of TO901317, production of VLDL particles increased as well.

Conclusions: LXR activation enhanced the expression of hepatic apoE, together with the alteration of lipoprotein particles produced from the differentiated hepatocyte-derived cells. HepG2 spheroids might serve as a good model of well-differentiated human hepatocytes for future investigations of hepatic lipid metabolism.

Keywords: Spheroid HepG2 cells, LXR agonist, Apolipoprotein E, ApoE rich HDL, VLDL

Background

Apolipoprotein E (apoE), a 34-kD glycoprotein produced mainly by hepatocytes and also secreted from several cells including macrophages and adipocytes, plays a crucial role in lipoprotein metabolism and atherosclerosis. It mediates the cellular uptake of several classes of lipoproteins by acting as a ligand for the chylomicron remnant receptor, the VLDL receptor, LDL receptor and the LDL receptor-related protein (LRP). ApoE produced by macrophages and those accessing macrophages from the bloodstream facilitate the reverse cholesterol transport by promoting the formation and maturation of HDL particles [1,2]. In addition to these functions, apoE produced in hepatocytes enhances the production of VLDL particles [3]. The increased production of hepatic VLDL particles, a phenomenon observed in insulin-resistant patients or some primary hyperlipidemia subjects, leads to the accumulation of atherogenic lipoproteins in the circulation resulting in the aggravation of atherosclerosis.

The genetic regulation of the apoE gene has been pursued extensively. Taylor et al has identified two hepatic enhancer elements located far-downstream of the apoE gene, and clarified the regions critical to the baseline expression of the apoE gene [4,5]. They also identified the duplicated downstream enhancer elements termed multienhancers (ME.1 and ME.2), and demonstrated that these elements are crucial for apoE expression in macrophages and adipocytes [6]. In addition, Laffitte

* Correspondence: kazuhisa-tky@umin.ac.jp
[1]Department of Metabolic Diseases, Graduate School of Medicine, The University of Tokyo, Tokyo 113-8655, Japan
Full list of author information is available at the end of the article

et al elegantly clarified that the nuclear receptor liver × receptor (LXR) regulates apoE expression in adipocytes and macrophages through direct interaction of the LXR response element found in both ME.1 and ME.2 [7].

In spite of these extensive analyses on apoE gene regulation, physiological factors which affect gene regulation of apoE in the liver have not been elucidated so far. Previous in vivo studies utilizing guinea pig [8] and cebus monkey [9] have shown that cholesterol feeding to these animals resulted in the up-regulation of apoE gene in the liver, raising the possibility that the accumulation of cholesterol in hepatocytes would affect hepatic up-regulation of the apoE gene. In addition, investigation in mice also indicated the up-regulation of hepatic apoE gene by cholesterol feeding [10]. However, the contribution of LXR in the regulation of murine hepatic apoE was not demonstrated [7,10]. Furthermore, no study has clarified the role of LXR in the regulation of hepatic apoE gene in human-derived hepatocytes or hepatic cell lines, with only one exception which utilized artificial reporter gene construct, in which ME.1 or ME.2 was placed just before the -890 to +93 apoE promoter [7].

As for the model of human hepatocytes, HepG2 cells have been widely used for in vitro experiments; however HepG2 cells grown in monolayer form on a culture plate are different from the in vivo hepatocytes which exist in three dimensional form in the liver, and would not completely reflect the physiological functions of hepatocytes. HepG2 cells in spheroid culture, which grow in three dimensional form after being encapsulated in alginate beads [11], have been shown to be more differentiated than HepG2 cells cultured in monolayer form; the cells proliferating in alginate beads form cell-cell contact with each other, and normal hepato-cellular junctional complexes including canaliculi with microvilli are constructed [11]. In consequence, the production of several proteins and the detoxificatory functions [11] as well as the production of cholesterol and triglycerides [12] increased significantly in HepG2 cells in spheroid culture compared to those in monolayer culture.

In this report, we first compared the production of several apolipoproteins from HepG2 cells in spheroid culture with those in monolayer culture. Next, we examined the effect of TO901317, a synthetic LXR ligand, on the secretion of apoE as well as lipoproteins with HepG2 cells cultured both in three-dimensional form and in monolayer form.

Results

HepG2 cells cultured in spheroid form (S-Hep) secreted more albumin and apolipoproteins than HepG2 cells cultured in monolayer (M-Hep)

HepG2 cells cultured in spheroid form grew in three dimensional form (Figure 1A). To validate the differentiation of HepG2 cells prepared as spheroids in our procedure, we first examined the time-course changes in the secretion of albumin. As shown in Figure 1B, the secretion of albumin from S-Hep was enhanced; the highest secretion level was observed on Day 11, reaching as high as 4.5-fold compared to M-Hep, which was concordant with the previous report [11]. The secretions of apolipoprotein A-I (apoA-I), apoE, and apolipoprotein B (apoB) did also increase in S-Hep, and the time-course changes in their levels were almost the same as those found with albumin (Figure 1C-E). The mRNA levels of apoA-I and apoE on Day 11 of S-Hep revealed a 3-fold and 3.5-fold increase compared to M-Hep (Figure 2A). Because the levels of albumin and apoE secretions were highest on Day 11, for the subsequent experiments, we utilized S-Hep on Day 11.

PPAR-α, PPAR-γ, LXR-α, RXR-α were more abundant in the nuclear fractions of S-Hep than in those of M-Hep

In order to elucidate whether the up-regulation of the genes of apolipoproteins in S-Hep were associated with changes in the nuclear receptors, we next examined the nuclear protein levels in S-Hep in comparison with M-Hep. As shown in Figure 2B and 2C, the Western blot analyses of the proteins prepared from nuclear fractions revealed that peroxisome proliferator-activated receptor (PPAR)-α, LXR-α and retinoid × receptor (RXR)-α were more abundant in S-Hep than M-Hep. We did not observe differences in nuclear protein levels of hepatocyte nuclear factor (HNF)1-α and HNF4-α between S-Hep and M-Hep, however, PPAR-γ was also increased in S-Hep. This result suggested that the state of differentiation of hepatic derived cells would affect the expressions of several proteins associated with lipid metabolism at the level of DNA transcription.

TO901317 increased apoE secretion and suppressed apoA-I secretion from HepG2 spheroids more evidently than monolayer HepG2 cells

The increased nuclear level of LXRα in S-Hep together with the increased secretion of apoE from S-Hep prompted us to evaluate the effect of LXRα agonist on the secretion of apoE, because LXRα has been identified as a critical factor for the regulation of apoE in macrophages and adipocytes. Thus we next examined the effect of TO901317 (TO), a synthetic LXRα agonist, on the apolipoproteins' secretion from S-Hep as well as M-Hep. As was shown in Figure 3A, the incubation of cells with TO did not alter the levels of apoB secretion in both S-Hep and M-Hep. The secretion of apoA-I was decreased in both forms of HepG2 cells when the cells were incubated with TO, which was concordant with the previous finding by Huuskonen et al (Figure 3B) [13]. On the other hand, apoE secretion was enhanced

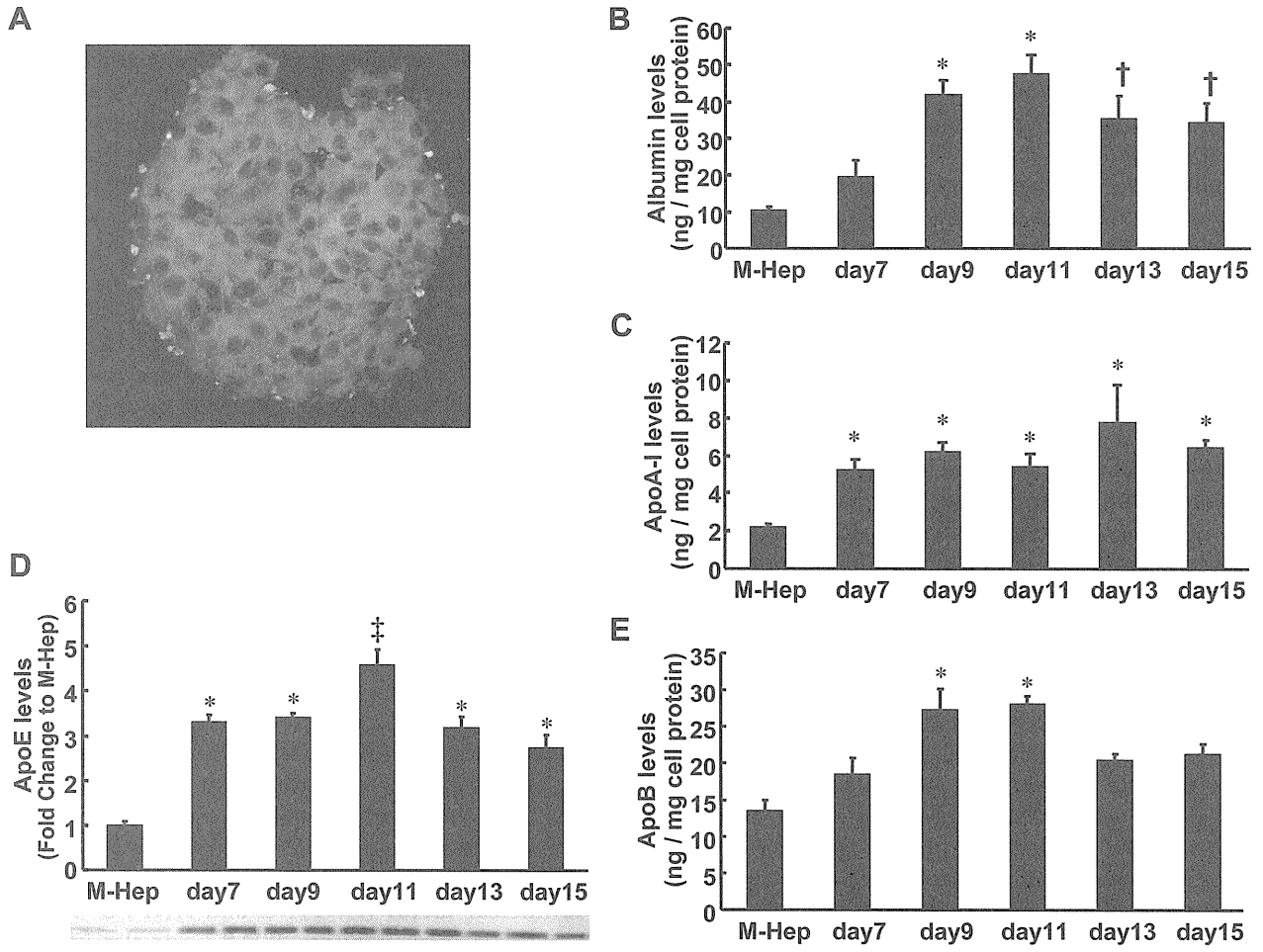

Figure 1 Differences in albumin and apolipoproteins secretion between monolayer and spheroid HepG2 cells. (A) Representative appearance of HepG2 spheroids on Day 11. HepG2 spheroids were fixed with 10% formalin solution, and examined with confocal microscopy. Briefly, from a single HepG2 cell, cells proliferate and form a spheroidal cell-cluster in an aliginate bead. (B-E) Time-course changes in the secretion of albumin (B), apoA-I (C), apoE (D), and apoB (E) from S-Hep cells. S-Hep (spheroid HepG2 cells) were prepared and grown in alginate beads as described in Materials and Methods, and the protein levels in the media on different time points after the beginning of the culture were measured. X axes represent the days after the beginning of S-Hep culture. Data are mean ± SEM (n = 4). *: $P < 0.01$ compared with M-Hep; †: $P < 0.03$ compared with M-Hep; ‡: $P < 0.01$ compared with M-Hep and $P < 0.03$ with S-Hep on the other time points.

not only in S-Hep but also in M-Hep with the incubation of cells with TO (Figure 3C). The induction of apoE in M-Hep plateaued at 0.02 μM TO, while the dose-dependent increase in apoE secretion from S-Hep was observed up to 0.2 μM. In addition, this incremental apoE secretion was more prominent in S-Hep, reaching almost twice the level of cells without TO.

TO901317 increased apoE and ABCA1 mRNA levels in HepG2 spheroids

In order to evaluate whether the increased secretion of apoE from S-Hep treated with TO was associated with the upregulation of the apoE gene, we examined the levels of apoE mRNA as well as ATP binding cassette transporter (ABC) A1 mRNA with quantitative real time PCR analyses. As shown in Figure 3D, the mRNA levels of apoE were significantly elevated by TO treatment, indicating that LXRα activated with TO would have increased the transcription of apoE in S-Hep. ABCA1, which is regulated by LXR, was also upregulated by TO901317, although the levels of the induction were less than those observed with apoE (Figure 3E).

Distribution of apoE secreted from S-Hep among lipoproteins

As shown in the above experiments, we confirmed that the secretion of apoE was enhanced in S-Hep compared to M-Hep, and treatment of HepG2 cells with TO resulted in the augmentation of apoE secretion from HepG2 cells. We next analyzed the distributions of

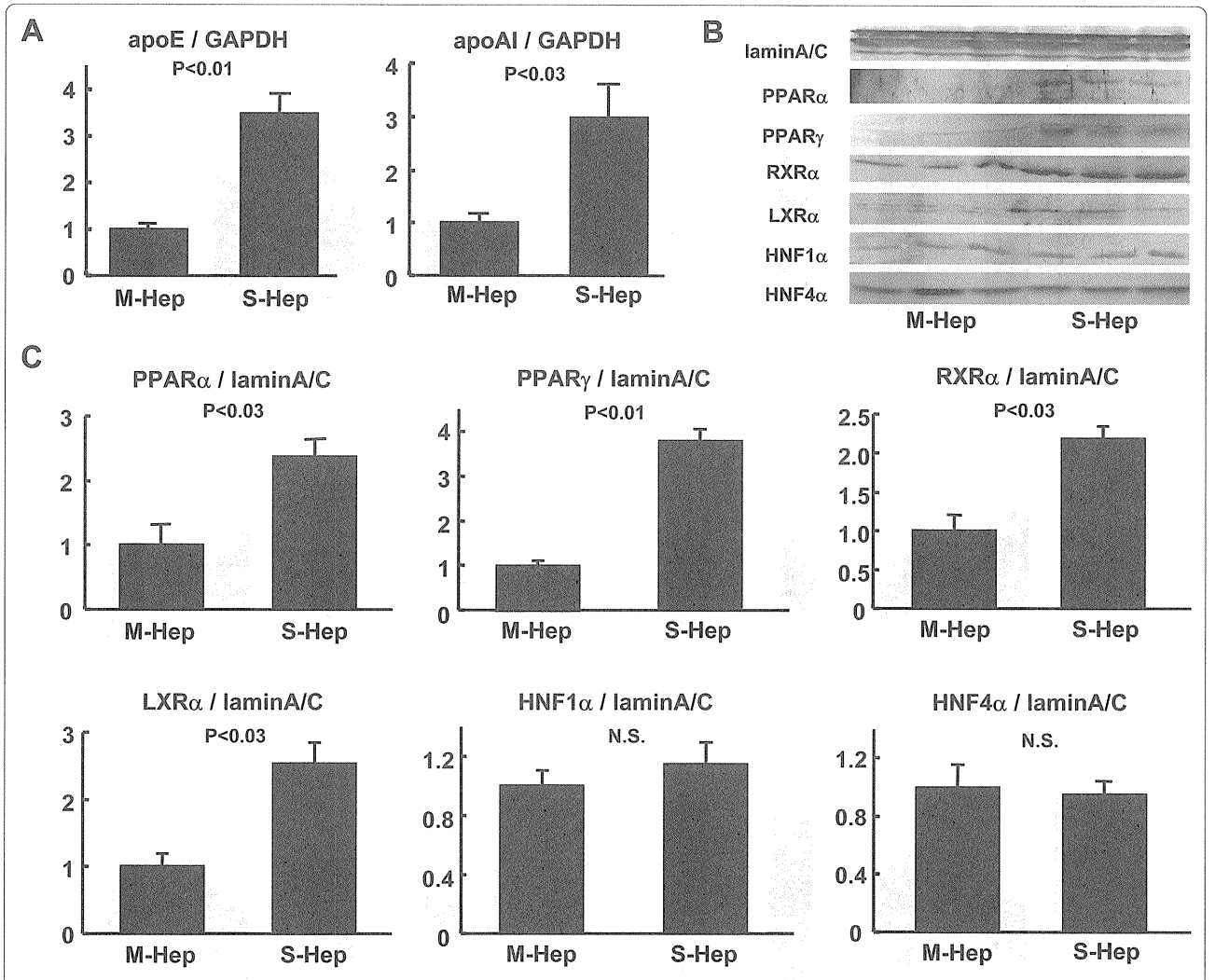

Figure 2 Differences in apolipoprotein mRNA and nuclear receptor protein levels among M-Hep and S-Hep. (A) Analyses of mRNA levels of apoE and apoA-I with quantitative RT-PCR (n = 4). GAPDH mRNA was used as the endogenous control for the expression levels of the gene of interest. (B, C) Western blot analyses were performed with the proteins prepared from nuclear fractions (Panel B), and nuclear protein levels were quantified with Image J utilizing lamin A/C as the internal control (Panel C) (n = 3). Y-axes in panels A and C represent ratios to the data of M-Hep.

apoE, together with those of apoB and apoA-I, among lipoproteins after fractionating the media with fast protein liquid chromatography (FPLC) which separated lipoproteins depending on their sizes. The results are shown in Figure 4 and 5: the fractions 21 - 26 corresponded to VLDL, fractions 29 - 37 to LDL, and fractions 38 - 48 to HDL based on the analysis of human plasma (data not shown). Both in S-Hep and M-Hep, apoA-I distribution was noted almost exclusively on fractions corresponding to HDL fractions, especially small HDL fractions; this distribution was not altered even with TO treatment. ApoB proteins were detected in fractions relevant to VLDL and LDL fractions, although the apoBs found in VLDL were scarce. In addition, no difference was observed in the distribution patterns of apoB between S-Hep and M-Hep, and treatment with TO did not alter these patterns. In contrast, unlike the findings of apoA-I and apoB, the distribution of apoE on lipoproteins was affected not only by the methods of the culture but also by the treatment with TO. ApoE secreted from M-Hep, regardless of the treatment with TO, were detected in the fractions spanning between those of LDL and HDL, suggesting its distribution on large HDL fractions; in addition, no apoE band was found in VLDL fractions even by the treatment with TO. On the other hand, the culture of HepG2 cells in spheroidal form rendered the apoE protein to reside on normal-sized HDL particles. Interestingly, treatment of S-Hep with TO not only increased the amount of secreted apoE incrementally with the increment of the

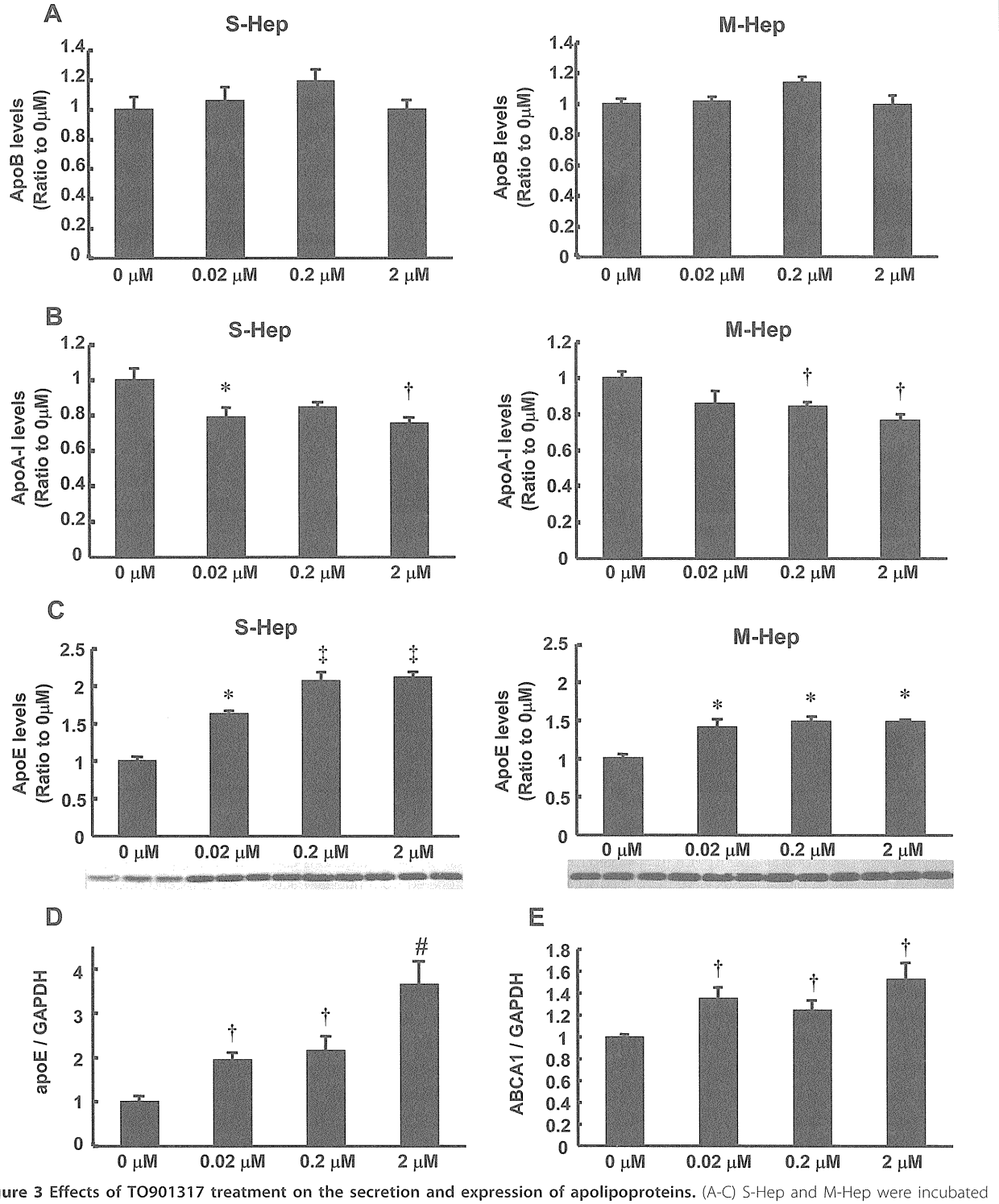

Figure 3 Effects of TO901317 treatment on the secretion and expression of apolipoproteins. (A-C) S-Hep and M-Hep were incubated with different concentration of TO901317, and the levels of apoipoproteins secreted in the medium were analyzed. Panel A, B and C represented apoB, apoA-I and apoE levels, respectively. (D, E) S-Hep were incubated with different concentration of TO901317, and mRNA levels of apoE (D) and ABCA1 (E) were analyzed. Data are mean ± SEM (n = 4). X-axes represent the concentration of TO901317. *: $P < 0.01$ compared with 0 μM, †: $P < 0.05$ with 0 μM, ‡: $P < 0.01$ with 0 and 0.02 μM, #: $P < 0.03$ with 0 and 0.02 μM.

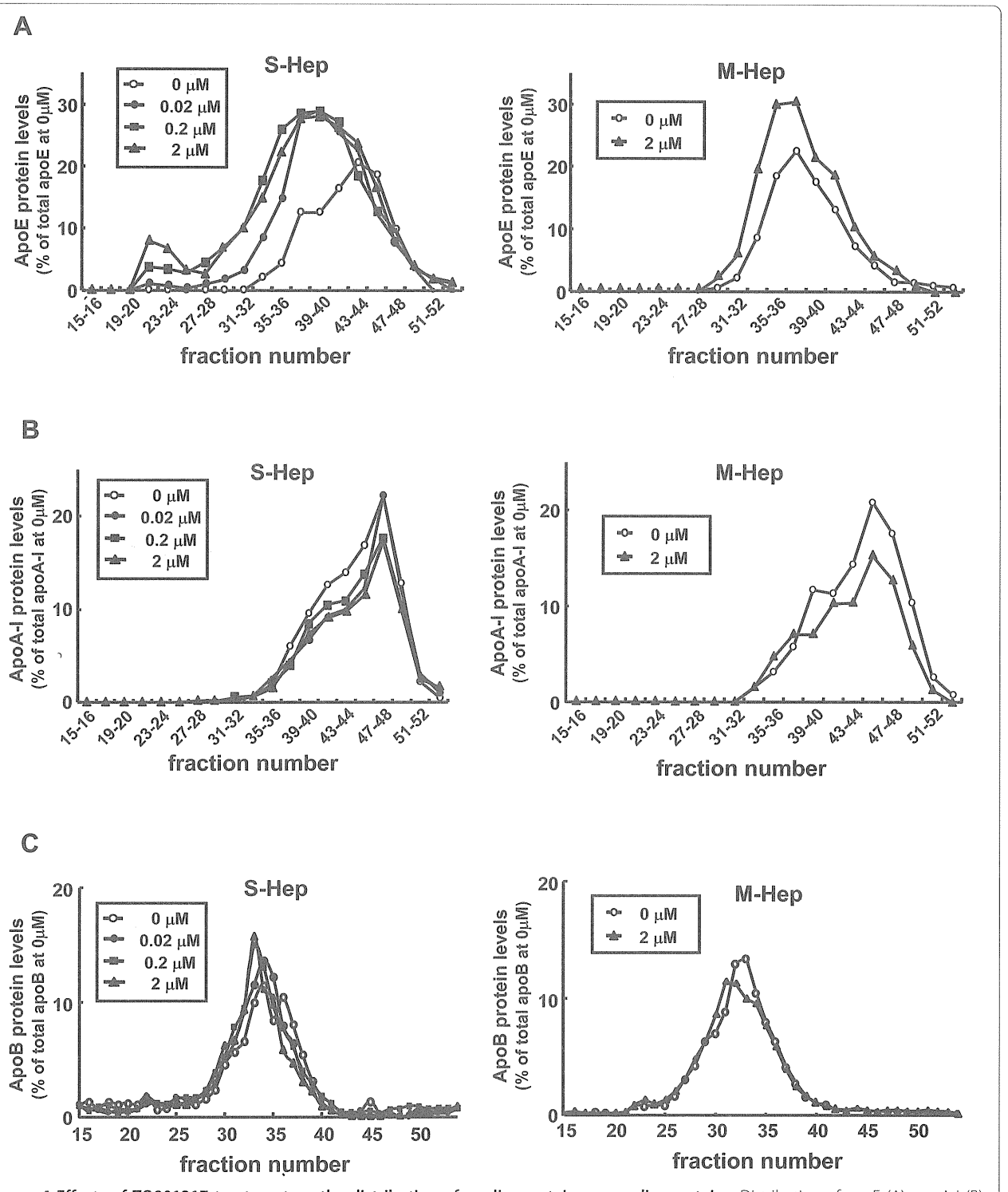

Figure 4 Effects of TO901317 treatment on the distribution of apolipoprotein among lipoproteins. Distribution of apoE (A), apoA-I (B), and apoB (C) on lipoprotein particles in the medium harvested from S-Hep (left) and M-Hep (right). Following the fractionation of the media with FPLC depending on the size of lipoproteins, fractionated samples were subjected to Western blot analyses or protein measurement with ELISA kits. White circles, black circles, squares and triangles represent the results from the medium of cells incubated with 0 μM, 0.02 μM, 0.2 μM and 2 μM of TO901317, respectively.

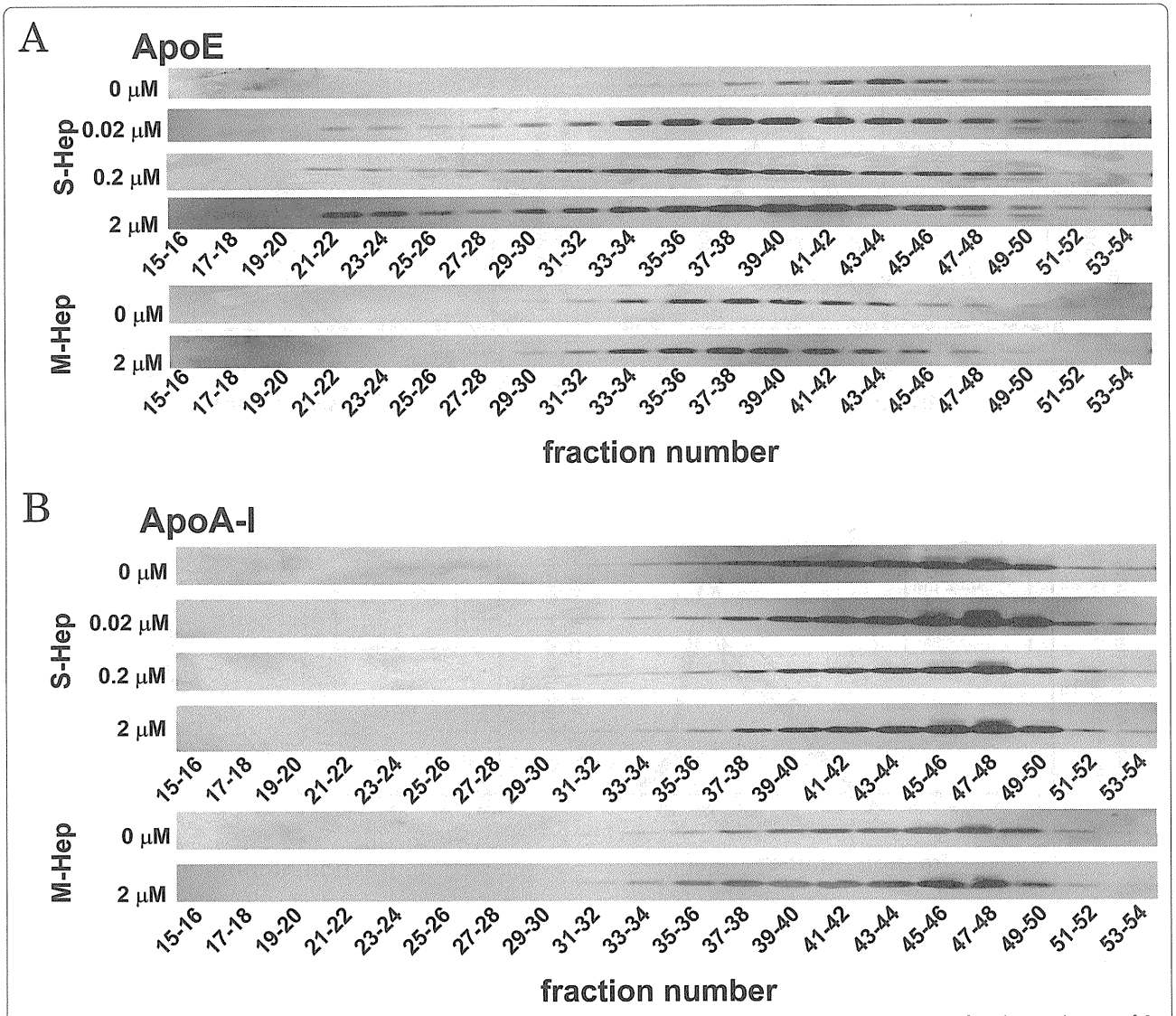

Figure 5 Western blot analyses on the distribution of apoE and apoA-I proteins among lipoprotein classes. After the incubation of S-Hep and M-Hep with TO901317 at the concentrations indicated, the media were fractionated with FPLC and the fractionated samples were subjected to Western blot analyses. Panel A and B represent the distributions of apoE and apoA-I, respectively.

dose of TO, but also rendered apoE to distribute on fractions larger than normal HDL. Based on the observation that neither apoA-I nor apoB was detected in these lipoprotein fractions, these fractions were assumed to be large apoE rich HDL. Furthermore, TO treatment of S-Hep resulted in the appearance of apoE on VLDL fractions; the amount of apoE on VLDL increased incrementally when the concentration of TO was increased up to 2 μM. In addition, as shown in Figure 6, treatment of S-Hep with 2 μM TO resulted in the increased triglycerides levels in the fractions where apoE protein increased with TO treatment. These results indicated that the TO treatment not merely resulted in the increased apoE protein levels in VLDL and large HDL fractions, but also resulted in the increased particle numbers and/or the enrichment of lipid content of VLDL and large HDL particles.

Discussion

Utilization of primary hepatocytes or hepatocyte-derived cell lines for in vitro experiments has helped us understand the lipid metabolism in the liver. However, it has been known that even the primary hepatocytes, when cultured in monolayer form, lose their differentiated, physiological functions quickly probably due to the loss of its three dimensional in vivo conformation in the experimental setting. In vivo experiments with rodents have also enabled us to elucidate the lipid metabolism

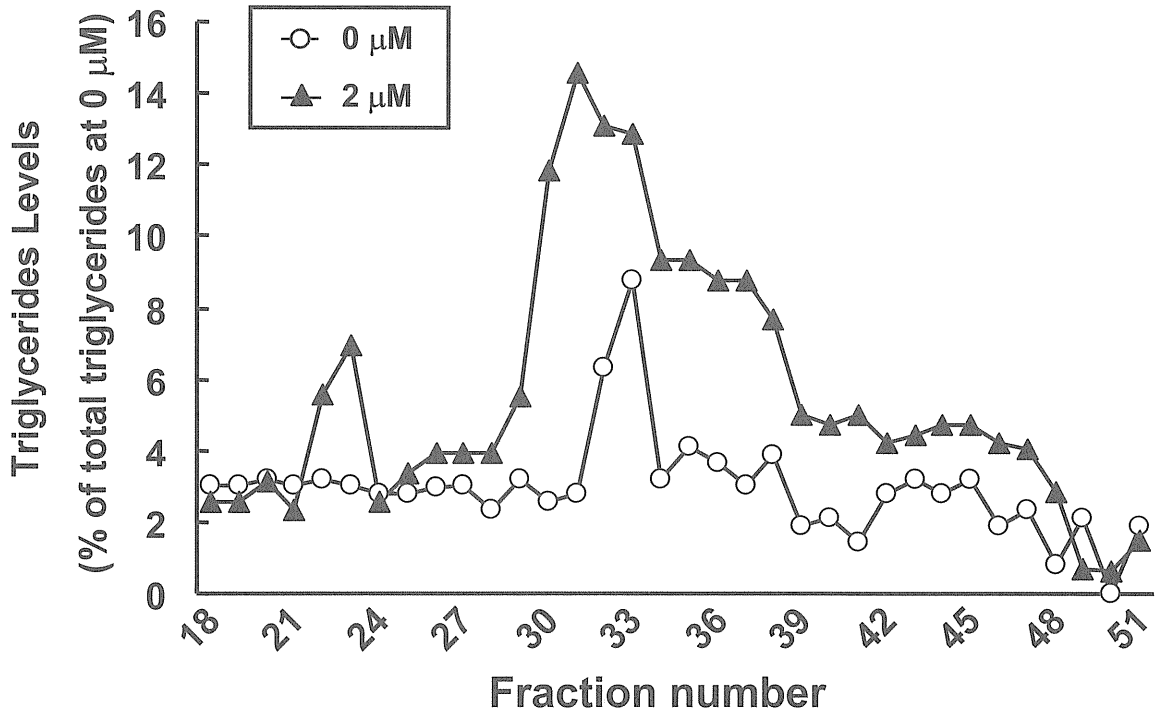

Figure 6 Analyses of triglyceride levels in the FPLC-fractionated samples. FPLC fractions obtained from S-Hep with or without 2 μM TO were subjected to the measurement of triglyceride (TG) levels with enzymatic method. White circles and triangles represent the results from the medium of cells incubated with 0 μM and 2 μM of TO901317, respectively.

in the liver; however, rodents might have been known to possess different properties from humans in lipid metabolism. Thus, in this study, in order to overcome these obstacles, we utilized 3-D spheroid culture system utilizing alginate beads, which has proven to be an easily-manipulative tactic to reproduce hepatocytes or hepatocytes-derived cells similar to their natural, differentiated in vivo counterparts.

Concordant with the previous observation by Khalil et al. [11], we were able to demonstrate that the culture of HepG2 cells in spheroid form resulted in enhanced albumin secretion compared to that in monolayer form, indicating that S-Hep utilized in this study had been more differentiated than M-Hep. The secretions of apoE, apoA-I, and apoB were also enhanced in S-Hep, and the nuclear protein contents of PPAR-α, PPAR-γ, LXR-α and RXR-α were increased in S-Hep, indicating that both of which are the features of differentiated hepatocytes or hepatocyte-derived cells. Furthermore, activation of LXR with TO901317 treatment of S-Hep resulted in the increased secretion of apoE protein which was accompanied by the up-regulation of apoE mRNA levels. Taking into account the previous study not showing a significant up-regulation of apoE gene with M-Hep treated with LXR activation [7], we assume that the differentiation of cells would be important to clearly examine the regulation of apoE gene in hepatocytes or hepatocyte-derived cells with LXR agonist, which is the case for macrophages and adipocytes [7].

The physiological regulation of apoE gene in the liver has so far not been clarified, although the baseline expression has been known to be controlled by distal hepatic enhancer elements [4,5] as well as the proximal promoter region to which TR4 orphan nuclear receptor binds [14]. Laffitte et al suggested that apoE enhancers and promoters containing LXRE would be important for the activation of apoE promoter in M-Hep; however, administration of LXR agonist in mice revealed a slight but non-significant role of LXR in the regulation of apoE in vivo [7]. Their observation does not depart at all from our present study, considering that murine lipid metabolism differs from that of humans in several respects. It is also plausible that factors other than LXR would regulate hepatic apoE gene in mice and probably in humans, considering that the degree of up-regulation of apoE gene observed in our study is less than those found in adipocytes and macrophages [7]. Further studies are needed to clarify these factors, and we believe that utilization of S-Hep would enable us to elucidate these factors.

In this study, we also found that the increased apoE secretion from S-Hep resulted in the alteration of

lipoprotein classes produced from the cells. One of the aspects of this alteration is the increased production of VLDL particles. In the state of hepatic steatosis, not only triglycerides but also cholesterol accumulate in hepatocytes [15], and the oxidative stress which increases in hepatic steatosis [16] transforms the cholesterol to oxysterol, which is a natural ligand for LXR. Because the production of apoE is one of the important determinants for the secretion of VLDL or VLDL-TG from the liver [3], the upregulation of apoE gene together with the increased production of triglycerides [17,18] by LXR activation facilitates the production of VLDL particles, resulting in the atherogenic lipid profile of the metabolic syndrome.

The other interesting finding in the alteration of lipoprotein production from S-Hep with TO901317 treatment was the increased production of large HDL particles containing apoE. Treatment with TO901317 prevented atherosclerosis in various mouse models [19-21], and increased apoE-rich HDL particles in C57BL6 mice [22,23]. These reagent effects have been attributed to the enhanced reverse cholesterol transport from macrophages [24] through the up-regulation of several key macrophagic proteins such as ABCA1 and apoE [25,26]. However, in this study, we did indicate that apoE-rich large HDL particles were also produced from the differentiated hepatocyte-derived cells, and that the induction was more pronounced with increasing increments of LXR activation. Although apoE-rich HDL has been speculated to play a role in delivering cholesterol to hormone-producing tissues such as adrenal tissues [27,28], several lines of study have indicated that apoE-rich HDL would also play an important role in reverse cholesterol transport; apoE-rich HDL is mainly contained in large HDL and large HDL has been demonstrated to extract cholesterol from macrophages [29]. It was also suggested that apoE-containing HDL efficiently enhanced cholesterol efflux [2,30]. Thus the increased production of apoE-rich large HDL particles from differentiated hepatocytes induced by LXR activation might have a role in the protection against atherosclerosis.

Conclusions

In summary, by utilizing the differentiated spheroid HepG2 cells, for the first time we were able to clearly demonstrate that LXR activation resulted in the up-regulation of human hepatic apoE, which also enhanced the production of VLDL particles and large apoE rich HDL particles. In future studies, investigation using HepG2 spheroids as surrogates to well-differentiated human hepatocytes would serve well as a model to precisely understand lipid metabolism in the liver.

Methods

Cell Culture and Experimental Protocol

HepG2 cells, purchased from American Type Culture Collection (ATCC, Manassas, VA), were cultured and maintained in DMEM (Sigma-Aldrich Co. St. Louis, MO) supplemented with 10% fetal bovine serum (FBS, Gibco BRL, Eggstein, Germany) and 1% penicillin/streptomycin (Gibco). For the experiment with M-Hep without TO (Sigma-Aldrich), 24 hours prior to the harvest of medium and cells, the medium was replaced with FBS-free medium to eliminate the plasma proteins derived from FBS in the medium. In the experimentation of M-Hep with TO, the medium was exchanged for that containing various concentrations of TO dissolved in DMSO at the cell confluency of around 70%. Two days later, the medium was replaced with the FBS-free medium containing the same concentration of TO, and cells were incubated for another 24 hours prior to the analysis. The collected cells were suspended in RIPA buffer (Santa Cruz Biotechnology, Santa Cruz, CA) for further analysis. The protein levels of the cell lysates were measured with Lowry methods (BioRad, Hercules, CA.) according to the manufacturer's protocol.

S-Hep were prepared following the methods described previously [11,12] with some modification. Briefly, HepG2 cells cultured in monolayer were detached completely with Trypsin-EDTA (Gibco) and suspended in α-MEM (Gibco) containing 10% FBS at the concentration of 0.5×10^6/mL. The medium containing HepG2 cells was mixed with the same amount of 2% alginate (Sigma). The mixed solution was dropped into 0.102 M $CaCl_2$/0.15 M NaCl (pH 7.4) solution at the speed of 1.5 ml/min through a 23 G cannula equipped inside another 19 G cannula from which the air was ejected at the speed of 1.2 L/min. This procedure yielded alginate-beads containing HepG2 cells, whose diameters ranged from 300 to 500 μm. The alginate beads were washed with DMEM twice and cultured in DMEM supplemented with 10% FBS and 1% penicillin/streptomycin. Prior to the harvest of cells and medium, beads containing S-Hep were washed twice with DMEM and cultured in FBS-containing DMEM with or without TO for two days. Thereafter, the medium was exchanged with FBS-free medium containing the same concentration of TO, and the cells were incubated for another 24 hours. Then the media were collected, and the cells were dissolved in RIPA buffer after releasing them from alginate beads with the incubation in PBS containing 4 mM EGTA (pH 7.4) for 10 minutes.

Quantification of Secreted Proteins in Medium

The concentrations of albumin, apoA-I and apoB in the media were measured by indirect sandwich enzyme-

linked immunosorbent assay (ELISA) with human albumin ELISA quantification kit (Bethyl laboratories, Inc. Montgomery, TX.) and ELISA kits for human apoA-I and apoB (Mabtech Inc. Nacka Strand, Sweden). For the quantification of apoE levels, the media, the volumes of which were adjusted according to cell protein levels, were subjected to 10% SDS-PAGE followed by Western-blot analysis with anti-apoE antibody (Chemicon International Inc, Temecula, CA), and the intensities of the bands were measured by Image J (from the NIH).

Preparation and Analysis of Nuclear Fraction

The nuclear fractions of HepG2 cells were obtained as follows: cells were dissolved in Buffer A (10 mM HEPES, 1.5 mM $MgCl_2$, 10 mM KCl, 0.5 mM DTT, 0.05% NP40, protease inhibitor cocktail (Roche, Mannheim, Germany), pH7.9) and incubated on ice for 10 minutes, centrifuged at 900 g for 10 minutes. The pellets were homogenized in Buffer B (5 mM HEPES. 1.5 mM $MgCl_2$, 0.2 M EDTA, 0.5 mM DTT, 26% glycerol, protease inhibitor cocktail, pH 7.9) supplemented with NaCl to the final concentration of 300 mM. Then, the solutions were centrifuged at 24,000 g for 20 minutes, and the supernatants were analyzed as the nuclear fractions of the cells. To quantify the levels of each nuclear protein, 30 μg of nuclear proteins extracted as above were subjected to 8% SDS-PGE followed by Western blot analyses with anti-Lamin A/C, anti-PPAR-α, anti-PPAR-γ, anti-RXR-α, anti-LXR-α, anti-HNF-1α, or anti-HNF-4α antibody (Santa Cruz Biotechnology).

Quantitative Real Time PCR

Total RNAs extracted from M-Hep and S-Hep with GenElute mammalian total RNA miniprep kit (Sigma-Aldrich) were subjected to reverse transcription with Superscript II enzyme (Invitrogen Co. Carlsbad, CA). Real-time quantitative PCR was performed with Light-Cycler system (Roche Diagnostics Basel, Switzerland). The expression levels of the gene of interest were normalized to those of the endogenous control GAPDH mRNA, and the amounts of target gene expressions were expressed as a ratio to those of control cells. The following primers were used: for GAPDH, forward 5' CCACTCCTCCACCTTTGA 3' and reverse 5' GTG GTCCAGGGGTCTTAC 3'; for apoA-I, forward 5' TGTCCCAGTTTGAAGGCT 3' and reverse 5' ATCC TTGCTCATCTCCTGC 3'; for apoE, forward 5' GGGT CGCTTTTGGGATTAC 3' and reverse 5' CAACT CCTTCATGGTCTCG 3'; for ABCA1, forward 5' AAATCCATTGTGGCTGC 3' and reverse 5' GGGA-GAGAGAGGTTGTGATAC 3'.

FPLC Analysis

The media of S-Hep or M-Hep, the total volumes of which were 12 mL, were concentrated to about 500 μl by centrifugation through Amicon Ultara-15 (Millipore Co., Bedford, MA). Then 200 μl of concentrated medium was separated by FPLC utilizing Superose 6 column. The levels of apoB in the separated fractions were analysed with ELISA method. For the analyses of apoE and apoA-I, the separated fractions were subjected to Western blots utilizing anti-apoE antibody and anti-apoA-I antibody (Chemicon). To raise the sensitivity of western blot analysis, after the incubation with primary antibodies, the membranes were incubated in biotin-conjugated anti-goat IgG antibody (Sigma) and then detected by Vecstatin ABC kit (Vector laboratories, Inc, Burlingame, CA). FPLC fractions obtained from S-Hep with or without 2 μM TO were subjected to the measurement of triglycerides (TG) levels with enzymatic method (WAKO Pure Chemical Industries, Osaka, Japan). To standardize the TG values among samples from with or without TO, the values obtained were adjusted utilizing the TG levels of the media which was corrected with cellular protein levels.

Statistical analysis

The results were expressed as mean ± SEM. Differences between two groups were evaluated with student's *t*-test, and the differences among more than assessed with one-way ANOVA, followed by multiple comparison tests. the *P* value less than 0.05 was deemed as statistically significant.

List of Abbreviations

apoA-I: apolipoprotein A-I; apoB: apolipoprotein B; apoE: apolipoprotein E; TO: TO901317; M-Hep: HepG2 cells cultured in monolayer; S-Hep: HepG2 cells cultured in spheroidal form; HNF: hepatocyte nuclear factor; LXR: liver × receptor; PPAR: peroxisome proliferator-activated receptor; RXR: retinoid × receptor; ABC: ATP-binding cassette transporter; FPLC: fast protein liquid chromatography; FBS: fetal bovine serum; ELISA: enzyme-linked immunosorbent assay.

Acknowledgements

This research was supported by Grant-In-Aid No. 20591079 (to KT) from the Japan Society for the Promotion of Science.

Author details

[1]Department of Metabolic Diseases, Graduate School of Medicine, The University of Tokyo, Tokyo 113-8655, Japan. [2]Department of Cardiovascular Medicine, Graduate School of Medicine, The University of Tokyo, Tokyo 113-8655, Japan. [3]Department of Infection Control and Prevention, Graduate School of Medicine, The University of Tokyo, Tokyo 113-8655, Japan. [4]Department of Gastroenterology, Graduate School of Medicine, The University of Tokyo, Tokyo 113-8655, Japan. [5]Department of Advanced Medical Science, The Institute of Medical Science, The University of Tokyo, Tokyo 108-8639, Japan. [6]Fourth Department of Internal Medicine, Mizonokuchi Hospital, Teikyo University School of Medicine, Kanagawa 213-8507, Japan. [7]Department of Metabolism, Diabetes and Nephrology, Preparatory Office for Aizu Medical Center, Fukushima Medical University, Fukushima 965-8555, Japan.

Authors' contributions

MK participated in study design, carried out experiments and data analysis, and drafted the initial manuscript. NaI and MH participated in several experiments. NOI participated in the real-time PCR study. KM and KK were involved in study design and drafting manuscript. KT conceived of the study, coordinated the study design and helped to draft the manuscript. All authors read and approved the final manuscript.

Competing interests

The authors declare that they have no competing interests.

Received: 8 July 2011 Accepted: 5 August 2011
Published: 5 August 2011

References

1. Zhang WY, Gaynor PM, Kruth HS: **Apolipoprotein E produced by human monocyte-derived macrophages mediates cholesterol efflux that occurs in the absence of added cholesterol acceptors.** *J Biol Chem* 1996, **271**:28641-6.
2. Hara M, Matsushima T, Satoh H, Iso-o N, Noto H, Togo M, Kimura S, Hashimoto Y, Tsukamoto K: **Isoform-dependent cholesterol efflux from macrophages by apolipoprotein E is modulated by cell surface proteoglycans.** *Arterioscler Thromb Vasc Biol* 2003, **23**:269-74.
3. Tsukamoto K, Maugeais C, Glick JM, Rader DJ: **Markedly increased secretion of VLDL triglycerides induced by gene transfer of apolipoprotein E isoforms in apoE-deficient mice.** *J Lipid Res* 2000, **41**:253-9.
4. Simonet WS, Bucay N, Lauer SJ, Taylor JM: **A far-downstream hepatocyte-specific control region directs expression of the linked human apolipoprotein E and C-I genes in transgenic mice.** *J Biol Chem* 1993, **268**:8221-9.
5. Allan CM, Taylor S, Taylor JM: **Two hepatic enhancers, HCR.1 and HCR.2, coordinate the liver expression of the entire human apolipoprotein E/C-I/C-IV/C-II gene cluster.** *J Biol Chem* 1997, **272**:29113-9.
6. Shih SJ, Allan C, Grehan S, Tse E, Moran C, Taylor JM: **Duplicated downstream enhancers control expression of the human apolipoprotein E gene in macrophages and adipose tissue.** *J Biol Chem* 2000, **275**:31567-72.
7. Laffitte BA, Repa JJ, Joseph SB, Wilpitz DC, Kast HR, Mangelsdorf DJ, Tontonoz P: **LXRs control lipid-inducible expression of the apolipoprotein E gene in macrophages and adipocytes.** *Proc Natl Acad Sci USA* 2001, **98**:507-12.
8. Driscoll DM, Mazzone T, Matsushima T, Getz GS: **Apoprotein E biosynthesis in the cholesterol-fed guinea pig.** *Arteriosclerosis* 1990, **10**:31-9.
9. Hennessy LK, Osada J, Ordovas JM, Nicolosi RJ, Stucchi AF, Brousseau ME, Schaefer EJ: **Effects of dietary fats and cholesterol on liver lipid content and hepatic apolipoprotein A-I, B, and E and LDL receptor mRNA levels in cebus monkeys.** *J Lipid Res* 1992, **33**:351-60.
10. Peet DJ, Turley SD, Ma W, Janowski BA, Lobaccaro JM, Hammer RE, Mangelsdorf DJ: **Cholesterol and bile acid metabolism are impaired in mice lacking the nuclear oxysterol receptor LXR alpha.** *Cell* 1998, **93**:693-704.
11. Khalil M, Shariat-Panahi A, Tootle R, Ryder T, McCloskey P, Roberts E, Hodgson H, Selden C: **Human hepatocyte cell lines proliferating as cohesive spheroid colonies in alginate markedly upregulate both synthetic and detoxificatory liver function.** *J Hepatol* 2001, **34**:68-77.
12. Damelin LH, Coward S, Choudhury SF, Chalmers SA, Cox IJ, Robertson NJ, Revial G, Miles M, Tootle R, Hodgson HJ, Selden C: **Altered mitochondrial function and cholesterol synthesis influences protein synthesis in extended HepG2 spheroid cultures.** *Arch Biochem Biophys* 2004, **432**:167-77.
13. Huuskonen J, Vishnu M, Chau P, Fielding PE, Fielding CJ: **Liver × receptor inhibits the synthesis and secretion of apolipoprotein A1 by human liver-derived cells.** *Biochemistry* 2006, **45**:15068-74.
14. Kim E, Yang Z, Liu NC, Chang C: **Induction of apolipoprotein E expression by TR4 orphan nuclear receptor via 5' proximal promoter region.** *Biochem Biophys Res Commun* 2005, **328**:85-90.
15. Cano A, Ciaffoni F, Safwat GM, Aspichueta P, Ochoa B, Bravo E, Botham KM: **Hepatic VLDL assembly is disturbed in a rat model of nonalcoholic fatty liver disease: is there a role for dietary coenzyme Q?** *J Appl Physiol* 2009, **107**:707-17.
16. Robertson G, Leclercq I, Farrell GC: **Nonalcoholic steatosis and steatohepatitis. II. Cytochrome P-450 enzymes and oxidative stress.** *Am J Physiol Gastrointest Liver Physiol* 2001, **281**:G1135-9.
17. Chisholm JW, Hong J, Mills SA, Lawn RM: **The LXR ligand T0901317 induces severe lipogenesis in the db/db diabetic mouse.** *J Lipid Res* 2003, **44**:2039-48.
18. Grefhorst A, Elzinga BM, Voshol PJ, Plosch T, Kok T, Bloks VW, van der Sluijs FH, Havekes LM, Romijn JA, Verkade HJ, Kuipers F: **Stimulation of lipogenesis by pharmacological activation of the liver × receptor leads to production of large, triglyceride-rich very low density lipoprotein particles.** *J Biol Chem* 2002, **277**:34182-90.
19. Verschuren L, de Vries-van der Weij J, Zadelaar S, Kleemann R, Kooistra T: **LXR agonist suppresses atherosclerotic lesion growth and promotes lesion regression in apoE*3Leiden mice: time course and mechanisms.** *J Lipid Res* 2009, **50**:301-11.
20. Peng D, Hiipakka RA, Dai Q, Guo J, Reardon CA, Getz GS, Liao S: **Antiatherosclerotic effects of a novel synthetic tissue-selective steroidal liver × receptor agonist in low-density lipoprotein receptor-deficient mice.** *J Pharmacol Exp Ther* 2008, **327**:332-42.
21. Terasaka N, Hiroshima A, Koieyama T, Ubukata N, Morikawa Y, Nakai D, Inaba T: **T-0901317, a synthetic liver × receptor ligand, inhibits development of atherosclerosis in LDL receptor-deficient mice.** *FEBS Lett* 2003, **536**:6-11.
22. Jiang XC, Beyer TP, Li Z, Liu J, Quan W, Schmidt RJ, Zhang Y, Bensch WR, Eacho PI, Cao G: **Enlargement of high density lipoprotein in mice via liver × receptor activation requires apolipoprotein E and is abolished by cholesteryl ester transfer protein expression.** *J Biol Chem* 2003, **278**:49072-8.
23. Cao G, Beyer TP, Yang XP, Schmidt RJ, Zhang Y, Bensch WR, Kauffman RF, Gao H, Ryan TP, Liang Y, Eacho PI, Jiang XC: **Phospholipid transfer protein is regulated by liver × receptors in vivo.** *J Biol Chem* 2002, **277**:39561-5.
24. Zanotti I, Poti F, Pedrelli M, Favari E, Moleri E, Franceschini G, Calabresi L, Bernini F: **The LXR agonist T0901317 promotes the reverse cholesterol transport from macrophages by increasing plasma efflux potential.** *J Lipid Res* 2008, **49**:954-60.
25. Beyea MM, Heslop CL, Sawyez CG, Edwards JY, Markle JG, Hegele RA, Huff MW: **Selective up-regulation of LXR-regulated genes ABCA1, ABCG1, and APOE in macrophages through increased endogenous synthesis of 24(S),25-epoxycholesterol.** *J Biol Chem* 2007, **282**:5207-16.
26. Levin N, Bischoff ED, Daige CL, Thomas D, Vu CT, Heyman RA, Tangirala RK, Schulman IG: **Macrophage liver × receptor is required for antiatherogenic activity of LXR agonists.** *Arterioscler Thromb Vasc Biol* 2005, **25**:135-42.
27. Hammami M, Meunier S, Maume G, Gambert P, Maume BF: **Effect of rat plasma high density lipoprotein with or without apolipoprotein E on the cholesterol uptake and on the induction of the corticosteroid biosynthetic pathway in newborn rat adrenocortical cell cultures.** *Biochim Biophys Acta* 1991, **1094**:153-60.
28. Kraemer FB: **Adrenal cholesterol utilization.** *Mol Cell Endocrinol* 2007, **265-266**:42-5.
29. Matsuura F, Wang N, Chen W, Jiang XC, Tall AR: **HDL from CETP-deficient subjects shows enhanced ability to promote cholesterol efflux from macrophages in an apoE- and ABCG1-dependent pathway.** *J Clin Invest* 2006, **116**:1435-42.
30. Krimbou L, Marcil M, Chiba H, Genest J Jr: **Structural and functional properties of human plasma high density-sized lipoprotein containing only apoE particles.** *J Lipid Res* 2003, **44**:884-92.

doi:10.1186/1476-511X-10-134
Cite this article as: Kurano *et al.*: LXR agonist increases apoE secretion from HepG2 spheroid, together with an increased production of VLDL and apoE-rich large HDL. *Lipids in Health and Disease* 2011 **10**:134.

Journal of Chromatography A, 1218 (2011) 3447–3452

Contents lists available at ScienceDirect

Journal of Chromatography A

journal homepage: www.elsevier.com/locate/chroma

Liquid chromatographic separation of proteins derivatized with a fluorogenic reagent at cysteinyl residues on a non-porous column for differential proteomics analysis

Akiyo Koshiyama[a], Tomoko Ichibangase[a], Kyoji Moriya[b], Kazuhiko Koike[c], Itaru Yazawa[d], Kazuhiro Imai[a,*]

[a] Research Institute of Pharmaceutical Sciences, Musashino University, 1-1-20 Shinmachi, Nishitokyo-shi, Tokyo 202-8585, Japan
[b] Department of Infection Control and Prevention, Graduate School of Medicine, University of Tokyo, 7-3-1 Hongo, Bunkyo-ku, Tokyo 113-8655, Japan
[c] Department of Internal Medicine, Graduate School of Medicine, University of Tokyo, 7-3-1 Hongo, Bunkyo-ku, Tokyo 113-8655, Japan
[d] Imtakt Corporation, Kyoto Research Park, Chudoji Minami, Shimogyo-ku, Kyoto 600-8813, Japan

ARTICLE INFO

Article history:
Received 1 February 2011
Received in revised form 24 March 2011
Accepted 26 March 2011
Available online 4 April 2011

Keywords:
FD–LC–MS/MS method
Non-porous column
Wide-pore column
Differential proteomics analysis
Hepatocarcinogenesis

ABSTRACT

A wide-pore (30 nm) reversed-phase column (Intrada WP-RP, particle size 3 μm) was recently utilized for protein separation in differential proteomics analysis with fluorogenic derivatization-liquid chromatography–tandem mass spectrometry (FD–LC–MS/MS), and exerted a tremendous effect on finding biomarkers (e.g., for breast cancer). Further high-performance separation is required for highly complex protein mixtures. A recently prepared non-porous small-particle reversed-phase column (Presto FF-C18, particle size: 2 μm) was expected to more effectively separate derivatized protein mixtures than the wide-pore column. A preliminary experiment demonstrated that the peak capacity of the former was threefold greater than that of the latter in gradient elution of a fluorogenic derivatized model peptide, calcitonin. The FD–LC–MS/MS method with a non-porous column was then optimized and applied to separate liver mitochondrial proteins that were not efficiently separated with the wide-pore column. As a result, high-performance separation of mitochondrial proteins was accomplished, and differential proteomics analysis of liver mitochondrial proteins in a hepatitis-infected mouse model was achieved using the FD–LC–MS/MS method with the non-porous column. This result suggests the non-porous small-particle column as a replacement for the wide-pore column for differential proteomics analysis in the FD–LC–MS/MS method.

1. Introduction

High-performance liquid chromatography (HPLC) has been used for separating highly complex mixtures of compounds, such as cell and tissue extracts. However, because efficient separation of intact proteins is difficult, one-dimensional (1D) or multidimensional (mD) HPLC is usually performed with peptides generated by digesting intact proteins in proteomics analysis (reviewed in Ref. [1]). In contrast, we have developed the first reproducible quantification method using 1D HPLC for proteomics analysis, called fluorogenic derivatization-liquid chromatography-tandem mass spectrometry (FD–LC–MS/MS) with a database-searching algorithm. Intact protein mixtures were first derivatized at cysteinyl residues with a fluorogenic reagent, followed by isolation with a wide-pore reversed-phase column, Intrada WP-RP (30 nm pore size and 3 μm particle) (Imtakt, Kyoto, Japan), digestion of the derivatized proteins, and identification of the isolated proteins [2]. Application to real biological samples indicated the appearance of more than 400 or 500 proteins on a chromatogram [3–7]. Differential proteomics analysis demonstrated the existence of many proteins related to an early stage of Parkinson's disease [3], developmental stages of hepatocarcinogenesis [4], metastatic or normal breast cancer cells [5], the aging of rat brain regions [6], and the running speed of horses [7].

Differential proteomics analysis of liver proteins between hepatitis C virus (HCV) core gene transgenic (Tg) and non-transgenic (NTg) mice indicated some disease-related proteins in the developmental stages of hepatocarcinogenesis [4]. Since many of those proteins were related to the function of mitochondrial events (e.g., respiration, electron-transfer system, and β-oxidation), we further performed differential proteomics analysis of liver mitochondrial proteins between Tg and NTg mice by FD–LC–MS/MS to clarify the role of mitochondrial proteins. In a preliminary experiment, however, it was difficult to separate the mitochondrial protein mixture

* Corresponding author. Tel.: +81 42 468 9787; fax: +81 42 468 9787.
E-mail address: k-imai@musashino-u.ac.jp (K. Imai).

0021-9673/$ – see front matter © 2011 Elsevier B.V. All rights reserved.
doi:10.1016/j.chroma.2011.03.070

effectively using the conventional wide-pore column that was used for the FD–LC–MS/MS method. Therefore, we searched for other columns that have higher-performance separation ability than the wide-pore column.

According to recent technical developments, the use of a stationary phase of small and non-porous particles (sub-2 μm) reduces eddy diffusion and mass-transfer resistance in the mobile phase more than porous particles [8]. Chong et al. used sub-2 μm non-porous particles for separating intact proteins in biological samples [9]. However, the reproducibility of the retention time of each protein was very low, probably due to the hydrophobicity of the intact proteins and the large amount of proteins provided for ultraviolet detection, which could prevent using a non-porous column for differential proteomics analysis. In contrast, with FD–LC–MS/MS, the non-porous column seems to be useful because the proteins are derivatized into less hydrophobic ones with the hydrophilic reagent, and one or two orders of magnitude less amount of proteins is sufficient for fluorescence detection than for ultraviolet detection.

Therefore, in this study, we applied a non-porous small-particle reversed-phase column (Presto FF-C18, 2 μm particle, Imtakt) to the FD–LC–MS/MS method. Based on an investigation of column lengths and flow rates for the non-porous column, the optimized FD–LC–MS/MS method was applied to liver mitochondrial proteomics analysis, resulting in high-performance separation of the mitochondrial proteins. This result suggested the non-porous small-particle column as a replacement for the wide-pore column in differential proteomics analysis utilizing the FD–LC–MS/MS method. Also, the result of liver mitochondrial proteomics analysis indicated proteins related to hepatocarcinogenesis; thus, the roles of proteins in hepatocarcinogenesis will be investigated.

2. Experimental

2.1. Reagents

For this study, 7-chloro-N-[2-(dimethylamino)ethyl]-2,1,3-benzoxadiazole-4-sulfonamide (DAABD-Cl) and Buffer Solution pH 8.7 (6 M Guanidine Hydrochloride) were obtained from Tokyo Chemical Industry (Tokyo, Japan). In addition, 3-[(3-cholamidopropyl)dimethylammonio]propanesulfonate (CHAPS) and ethylenediamine-N,N,N′,N′-tetraacetic acid disodium salt (Na_2EDTA) were obtained from Dojindo Laboratories (Kumamoto, Japan). Tris(2-carboxyethyl)phosphine hydrochloride (TCEP) and β-lactoglobulin (M.W. 18,363) were purchased from Sigma–Aldrich (St. Louis, MO, USA). Calcitonin (M.W. 3,418) was purchased from Peptide Institute (Osaka, Japan). Trifluoroacetic acid (TFA) was obtained from Wako Pure Chemical Industries (Osaka, Japan). Acetonitrile (HPLC grade) was obtained from Kanto Chemical (Tokyo, Japan). All the other reagents were of analytical reagent grade and were used without further purification. Water was used after purification with the Milli-Q system (Nihon Millipore, Tokyo, Japan).

2.2. Columns

Non-porous spherical silica (2 μm particle and 2 m^2/g specific surface area) was utilized as packing material in the Presto FF-C18 column (Fig. 1) (Imtakt, Kyoto, Japan). Octadecylsilane (ODS) binds to functional groups on packing materials, indicating that Presto FF-C18 is useful for reversed-phase separation in HPLC. However, wide-pore spherical silica (30 nm pore size, 3 μm particle, and 100 m^2/g specific surface area) was utilized in the Intrada WP-RP column (Imtakt). Reversed-phase ligands exist on the surface of the packing materials of Intrada WP-RP, which was used as a conventional protein separation column for the FD–LC–MS/MS method. Presto FF-C18 columns were adopted with 4.6 mm i.d. and 50–250 mm length, while Intrada WP-RP with 4.6 mm i.d. and 250 mm length was usually utilized for protein separation [2–7].

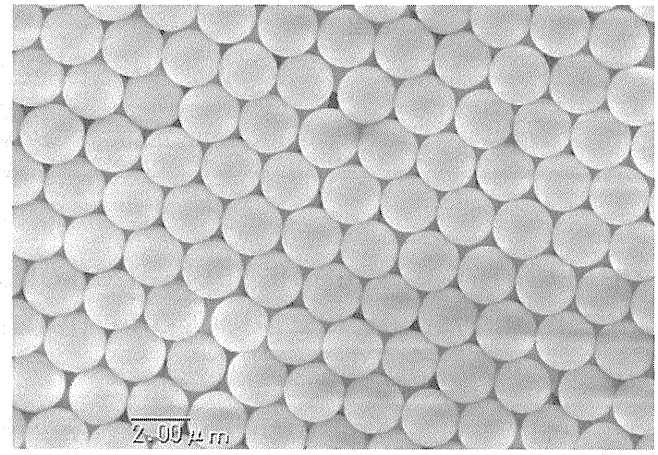

Fig. 1. Electron microscopic image of non-porous spherical silica (2 μm particle) utilized as a packing material in a Presto FF-C18 column.

2.3. FD reaction and separation of DAABD-calcitonin on the non-porous or the wide-pore column

A 10 μL aliquot of 5 μM calcitonin (Peptide Institute, Osaka, Japan) was mixed with 60 μL of 16.7 mM CHAPS/3.33 mM Na_2EDTA/0.833 mM TCEP in 6 M guanidine buffer (pH 8.7), 25 μL of 6 M guanidine buffer (pH 8.7), and 5.0 μL of 140 mM DAABD-Cl in acetonitrile. Each reaction mixture was incubated at 40 °C for 10 min, and the reaction was stopped with 3.0 μL of 20% TFAaq. The reaction mixture was then diluted three-fold with the mobile phase. A 10 μL aliquot of the diluted reaction mixture was injected into an HPLC system that consisted of a pump (L-2100, Hitachi) and a fluorescence detector (L-2485, Hitachi). Fluorescence detection was carried out at 505 nm (excitation at 395 nm). Separation was performed on the non-porous column (4.6 i.d. × 50, 100, 150, or 250 mm) or the wide-pore column (4.6 i.d. × 250 mm) (Imtakt, Kyoto, Japan). The column temperature was set at 60 °C, and the flow rate was 0.2–0.5 mL/min. The gradient elution was 10–40% B over 60 min ((A) water:acetonitrile:TFA = 90:10:0.10, v/v/v; (B) water:acetonitrile:TFA = 30:70:0.20, v/v/v).

2.4. Preparation of liver mitochondrial sample and determination of total proteins

Sixteen-month-old Tg and NTg mice were used for analysis. Progression of disease state and morphological features were described in previous reports [4,10].

A preliminary study clearly indicated that an extraction procedure utilizing a mitochondrial isolation commercial kit was not useful, due to the low repeatability in isolation handling. Therefore, in this study, mitochondria were extracted from liver samples (100 mg) by density-gradient centrifugation using a mannitol/sucrose solution, as reported by Lopez et al. [11]. The mitochondrial pellet obtained was suspended with twice-volume of 2% CHAPS in 6 M guanidine buffer (pH 8.7). The suspension was sonicated for 15 s on ice four times at 15 s intervals. The sonicated suspension was centrifuged at 13,000 g for 2 min at 4 °C. The supernatant was then collected and stored as a soluble fraction at −80 °C after freezing with liquid nitrogen. The total liver mitochondrial proteins were determined with a BCA™ Protein Assay